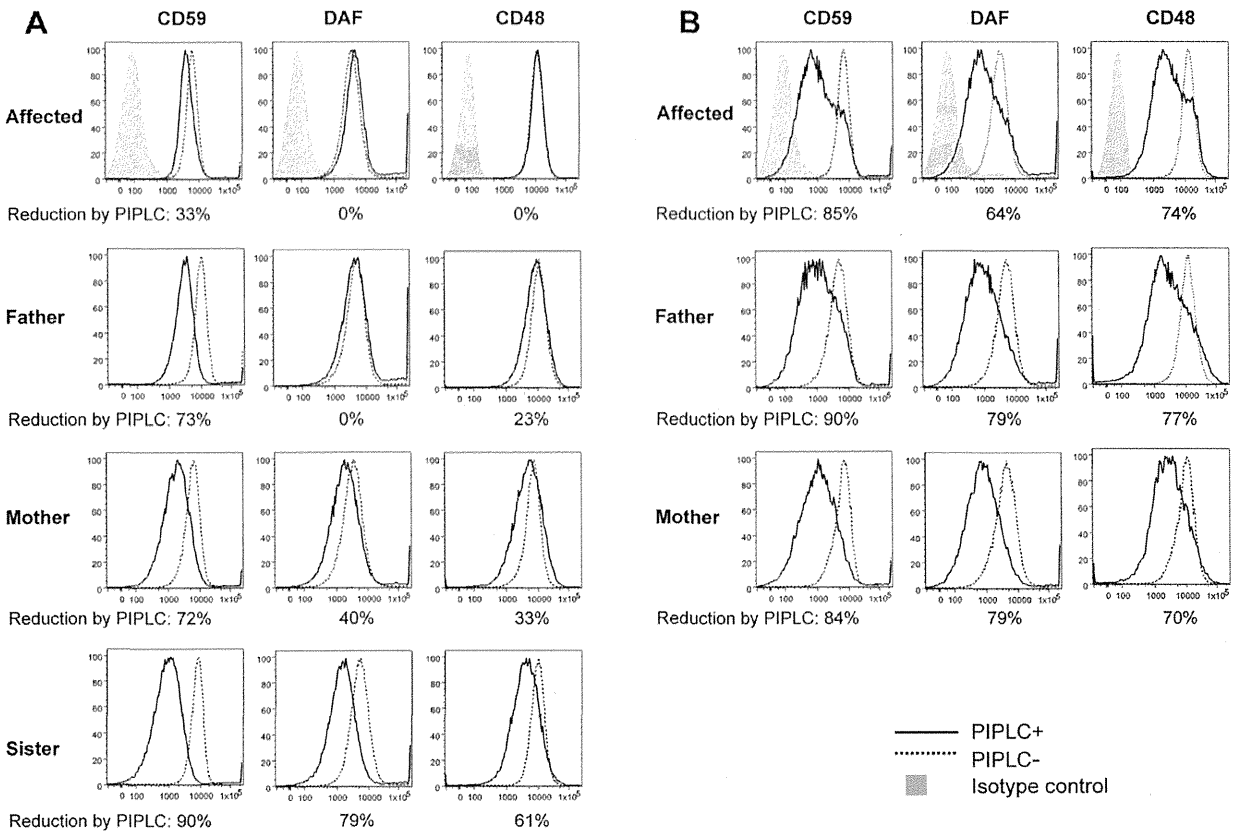

Figure 3. FACS analysis of GPI-APs on LCLs and their PI-PLC sensitivity. (A, B) Cells from one of the affected siblings (III-3) and the parents were transfected with empty pMEoriP vector (A) and pMEoriP-FLAG-humanPGAP1 (B). Cells from the healthy sister were used without transfection. Four days after transfection, cells were treated with (solid lines) or without (dotted lines) 10 unit/ml of PI-PLC for 1.5 h at 37°C, and the surface expression of CD59, DAF and CD48 were assessed by flow cytometry.
doi:10.1371/journal.pgen.1004320.g003

SureSelect Human All Exon Kit, which targets approximately 50 Mb of human genome (Agilent, Santa Clara, Ca, USA) and paired-end sequenced on a SOLiD 5500 xl instrument (Life Sciences, Carlsbad, CA, U.S.A.). Image analysis and base calling was performed using the SOLiD instrument control software with default parameters. Read alignment was performed with LifeScope 2.5 using the default parameters with human genome assembly hg19 (GRCh37) as reference. Single-nucleotide variants and small insertions and deletions (indels) were detected using LifeScope, GATK 2 and samtools/bcftools [37,38]. To replicate the results, DNA from individuals III-2 and III-3 was amplified using the Ion AmpliSeq Exome Kit (Life Technologies, Carlsbad, CA, U.S.A.) which targets approximately 58 Mb of the human genome. After quality control on the Bioanalyzer High Sensitivity Chip (Agilent, Santa Clara, Ca, USA) and emulsion PCR (Ion PI Template OT2 200 Kit v3, Life Technologies, Carlsbad, CA, U.S.A.) the samples were sequenced on a Proton PI chip Version 2 (Life Technologies, Carlsbad, CA, U.S.A.). Base calling, pre-processing of the reads, short read alignment and variant calling was performed using the Torrent Suite including the Torrent Variant Caller (TVC, Version 4.0) with default parameters recommended for the Ampliseq Exome panel (low stringency calling of germline variants, Version September 2013). Variant annotation was performed using Annovar, integrating data from a variety of public databases [39,40]. Additionally, variants were compared to an in-house database containing more than 350 sequenced exomes to identify further common variants which are not present in public databases. Finally, the variants were validated by PCR and Sanger sequencing according to the standard protocols to exclude technical artifacts and to test for segregation.

PI-PLC treatment and FACS analysis

Heparin blood samples were collected from one affected and from all unaffected siblings and parents. Lymphoblastoid Cell lines (LCLs) were generated and cultured in RPMI 1640 (Gibco, Life technologies, Darmstadt, Germany) that is supplemented with 10% FCS (PAA Biotech, Cölbe, Germany) and different other supplements. LCLs from one of the affected siblings (III-3) and the parents were transfected with empty pMEoriP vector or pMEoriP-FLAG-humanPGAP1. Cells from healthy sister were used without transfection. Cells (5×10^6) were suspended in 0.8 ml of Opti-MEM and electroporated with 20 µg each of the plasmids at 260 V and 960 µF using a Gene Pulser (Bio Rad, Hercules, CA). Four days after transfection, cells were treated with or without 10 unit/ml of PI-PLC (Molecular probes, Eugene, OR) for 1.5 h at 37°C. Surface expression of GPI-APs was determined by staining cells with mouse anti-human CD59 (5H8), -human DAF (IA10), -human CD48 (BJ40) antibodies and each isotype IgG followed by a PE-conjugated anti-mouse IgG antibody (BJ40, mouse IgG1 and IgG2a, and secondary antibody were purchased from BD

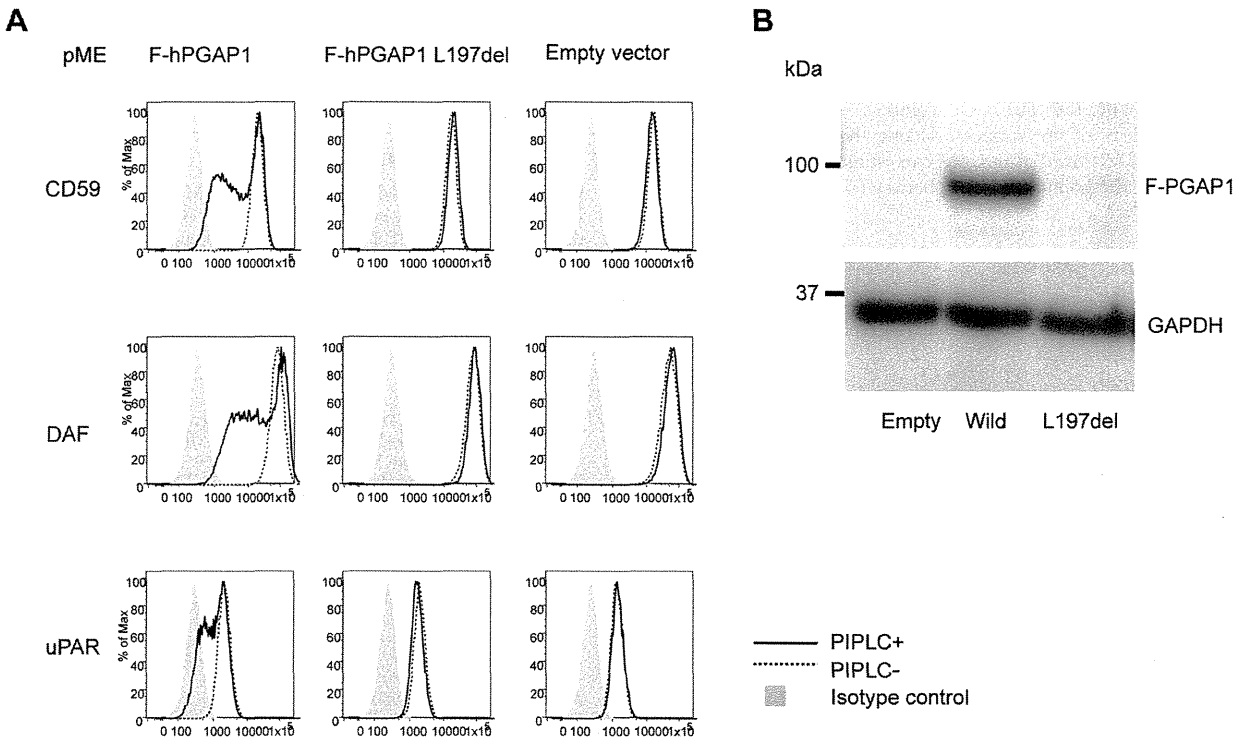

Figure 4. Functional ability of mutant *PGAP1* cDNA. (A) *PGAP1* deficient CHO cell (C10) [4] were transiently transfected with N-terminally-FLAG-tagged wild-type and mutant (L197del) human *PGAP1* driven by a strong promoter SRa, or an empty vector. Four days after transfection, each transfectant was treated with (solid lines) or without (dotted lines) 10 unit/ml of PI-PLC for 1.5 h at 37°C and the surface expression of CD59, DAF and uPAR were assessed by flow cytometry. (B) Two days after transfection of each *PGAP1* construct, lysates were immunoprecipitated with anti-FLAG beads and analyzed by SDS-PAGE/Western blotting. L197del mutant protein was not detected at all.
doi:10.1371/journal.pgen.1004320.g004

Biosciences, Franklin Lakes, NJ) and analyzed by flow cytometer (Cant II; BD Biosciences) using Flowjo software (Tommy Digital Inc., Tokyo, Japan).

Functional analysis using CHO cells

pMEFLAG-hPGAP1 mutant (L197del) bearing patient's mutation was generated by site directed mutagenesis. *PGAP1* deficient CHO cell (C10) [4] were transiently transfected with wild type or mutant pMEFLAG-hPGAP1 by electroporation. Cells (10^7) were suspended in 0.4 ml of Opti-MEM and electroporated with 20 μg each of the plasmids at 260 V and 960 μF using a Gene Pulser. Four days after transfection, cells were treated with or without 10 unit/ml of PI-PLC for 1.5 h at 37°C. Surface expression of GPI-APs was determined by staining cells with mouse anti-human CD59 (5H8), -human DAF (IA10), -hamster uPAR (5D6) antibodies and each isotype IgG, followed by a PE-conjugated anti-mouse IgG antibody and analyzed by flow cytometer using Flowjo software. Two days after transfection of each *PGAP1* construct, lysates were immunoprecipitated with anti-FLAG beads and analyzed by SDS-PAGE/Western blotting.

Web resources

1000Genomes, http://www.1000genomes.org/

ABI, L.T. (2012). LifeScope.: http://www.lifetechnologies.com/lifescope.

ANNOVAR: http://www.openbioinformatics.org/annovar/

GeneTalk: http://www.gene-talk.de

BWA, Burrows-Wheeler Aligner; http://bio-bwa.sourceforge.net/

dbSNP, NCBI: http://www.ncbi.nlm.nih.gov/snp/

GATK 2, Genome Analysis Toolkit: http://www.broadinstitute.org/gatk/index.php

Kyoto Encyclopedia of Genes and Genomes, KEGG, http://www.genome.jp/kegg/

MutationTaster: http://www.mutationtaster.org/ELAND, alignment algorithm, Illumina.com

NHLBI Exome Sequencing Project (ESP): http://evs.gs.washington.edu/EVS/

Online Mendelian Inheritance in Man (OMIM): http://www.omim.org

PolyPhen2: http://genetics.bwh.harvard.edu/pph2/

SIFT: http://sift.jcvi.org/

UCSC Genome Browser: www.genome.ucsc.edu

Supporting Information

Figure S1 Functional ability of mutant *PGAP1* cDNA. *PGAP1* deficient CHO cell (C10) [4] were transiently transfected with N-terminally-FLAG-tagged wild-type and mutant (Lys111Glu, Gln585Glu) human *PGAP1* or an empty vector driven by a strong promoter SRα (pME) or a weak promoter containing only TATA box (pTal). Four days after transfection, each transfectant was treated with (solid lines) or without (dotted lines) 10 unit/ml of PI-PLC for 1.5 h at 37°C and the surface expression of CD59 was assessed by flow cytometry.
(JPG)

Table S1 A list of all ESP database variants with a possible pathogenic effect (i. e. coding or at splice sites). We undertook further in silico analyses using MutationTaster and SIFT and presented in the last two columns estimations about the pathogenicity of the variants. Taking those estimations and the number of identified alleles, one can estimate the prevalence of the disease in the population to be between 7 and 13 per million. (PDF)

Acknowledgments

We are grateful to the families involved in this study for their participation. We thank Karen Toma, Petra Rothe, Heike Friebel-Stange, and Angelika Diem from Erlangen for assistance with LCLs, SNP array genotyping, and NGS. We also thank Mandy Krumbiegel for her support in establishing new NGS methods. We thank Kana Miyanagi from Osaka University for functional analysis.

Author Contributions

Conceived and designed the experiments: YMu AR TK RAJ YMa. Performed the experiments: YMu RB FR HT SS MA HS CB. Analyzed the data: YMu RB FR HT HS RAJ CB. Contributed reagents/materials/analysis tools: SS MA HS YMa. Wrote the paper: YMu TK RAJ.

References

1. Tiede A, Bastisch I, Schubert J, Orlean P, Schmidt RE (1999) Biosynthesis of glycosylphosphatidylinositols in mammalian and unicellular microbes. Biol Chem 380: 503–523.
2. McConville MJ, Menon AK (2000) Recent developments in the cell biology and biochemistry of glycosylphosphatidylinositol lipids. Mol Membr Biol 17: 1–16.
3. Fujita M, Kinoshita T (2012) GPI-anchor remodeling: potential functions of GPI-anchors in intracellular trafficking and membrane dynamics. Biochim Biophys Acta 1821: 1050–1058.
4. Tanaka S, Maeda Y, Tashima Y, Kinoshita T (2004) Inositol deacylation of glycosylphosphatidylinositol-anchored proteins is mediated by mammalian PGAP1 and yeast Bst1p. J Biol Chem 279: 14256–14263.
5. Fujita M, Maeda Y, Ra M, Yamaguchi Y, Taguchi R, et al. (2009) GPI glycan remodeling by PGAP5 regulates transport of GPI-anchored proteins from the ER to the Golgi. Cell 139: 352–365.
6. Tashima Y, Taguchi R, Murata C, Ashida H, Kinoshita T, et al. (2006) PGAP2 is essential for correct processing and stable expression of GPI-anchored proteins. Mol Biol Cell 17: 1410–1420.
7. Maeda Y, Tashima Y, Houjou T, Fujita M, Yoko-o T, et al. (2007) Fatty acid remodeling of GPI-anchored proteins is required for their raft association. Mol Biol Cell 18: 1497–1506.
8. Almeida AM, Murakami Y, Baker A, Maeda Y, Roberts IA, et al. (2007) Targeted therapy for inherited GPI deficiency. N Engl J Med 356: 1641–1647.
9. Johnston JJ, Gropman AL, Sapp JC, Teer JK, Martin JM, et al. (2012) The phenotype of a germline mutation in PIGA: the gene somatically mutated in paroxysmal nocturnal hemoglobinuria. Am J Hum Genet 90: 295–300.
10. van der Crabben SN, Harakalova M, Brilstra EH, van Berkestijn FM, Hofstede FC, et al. (2013) Expanding the spectrum of phenotypes associated with germline PIGA mutations: A child with developmental delay, accelerated linear growth, facial dysmorphisms, elevated alkaline phosphatase, and progressive CNS abnormalities. Am J Med Genet A 164: 29–35.
11. Swoboda KJ, Margraf RL, Carey JC, Zhou H, Newcomb TM, et al. (2013) A novel germline PIGA mutation in Ferro-Cerebro-Cutaneous syndrome: A neurodegenerative X-linked epileptic encephalopathy with systemic iron-overload. Am J Med Genet A 164: 17–28.
12. Krawitz PM, Murakami Y, Hecht J, Kruger U, Holder SE, et al. (2012) Mutations in PIGO, a member of the GPI-anchor-synthesis pathway, cause hyperphosphatasia with mental retardation. Am J Hum Genet 91: 146–151.
13. Krawitz PM, Schweiger MR, Rodelsperger C, Marcelis C, Kolsch U, et al. (2010) Identity-by-descent filtering of exome sequence data identifies PIGV mutations in hyperphosphatasia mental retardation syndrome. Nat Genet 42: 827–829.
14. Horn D, Wieczorek D, Metcalfe K, Baric I, Palczac L, et al. (2013) Delineation of PIGV mutation spectrum and associated phenotypes in hyperphosphatasia with mental retardation syndrome. Eur J Hum Genet doi:10.1038/ejhg.2013.241.
15. Kuki I, Yukitoshi Takahashi, Shin Okazaki, Hisashi Kawawaki, Eiji Ehara, Norimitsu Inoue, Taroh Kinoshita and Yoshiko Murakami (2013) Case report on vitamin B6 responsive epilepsy due to inherited GPI deficiency. Neurology 81: 1467–1469.
16. Nakamura K, Osaka H, Murakami Y, Anzai R, Nishiyama K, et al. (2014) PIGO mutations in intractable epilepsy and severe developmental delay with mild elevation of alkaline phosphatase levels. Epilepsia 55 (2): e13–e17.
17. Maydan G, Noyman I, Har-Zahav A, Neriah ZB, Pasmanik-Chor M, et al. (2011) Multiple congenital anomalies-hypotonia-seizures syndrome is caused by a mutation in PIGN. J Med Genet 48: 383–389.
18. Ohba C, Okamoto N, Murakami Y, Suzuki Y, Tsurusaki Y, et al. (2013) PIGN mutations cause congenital anomalies, developmental delay, hypotonia, epilepsy, and progressive cerebellar atrophy. Neurogenetics doi: 10.1007/s10048-013-0384-7.
19. Ng BG, Hackmann K, Jones MA, Eroshkin AM, He P, et al. (2012) Mutations in the glycosylphosphatidylinositol gene PIGL cause CHIME syndrome. Am J Hum Genet 90: 685–688.
20. Kvarnung M, Nilsson D, Lindstrand A, Korenke GC, Chiang SC, et al. (2013) A novel intellectual disability syndrome caused by GPI anchor deficiency due to homozygous mutations in PIGT. J Med Genet 50: :521–528.
21. Hansen L, Tawamie H, Murakami Y, Mang Y, Ur Rehman S, et al. (2013) Hypomorphic Mutations in PGAP2, Encoding a GPI-Anchor-Remodeling Protein, Cause Autosomal-Recessive Intellectual Disability. Am J Hum Genet 92: 575–583.
22. Krawitz PM, Murakami Y, Riess A, Hietala M, Kruger U, et al. (2013) PGAP2 Mutations, Affecting the GPI-Anchor-Synthesis Pathway, Cause Hyperphosphatasia with Mental Retardation Syndrome. Am J Hum Genet 92: 584–589.
23. Murakami Y, Kanzawa N, Saito K, Krawitz PM, Mundlos S, et al. (2012) Mechanism for release of alkaline phosphatase caused by glycosylphosphatidylinositol deficiency in patients with hyperphosphatasia mental retardation syndrome. J Biol Chem 287: 6318–6325.
24. Abou Jamra R, Wohlfart S, Zweier M, Uebe S, Priebe L, et al. (2011) Homozygosity mapping in 64 Syrian consanguineous families with non-specific intellectual disability reveals 11 novel loci and high heterogeneity. Eur J Hum Genet 19: 1161–1166.
25. Abou Jamra R, Philippe O, Raas-Rothschild A, Eck SH, Graf E, et al. (2011) Adaptor protein complex 4 deficiency causes severe autosomal-recessive intellectual disability, progressive spastic paraplegia, shy character, and short stature. Am J Hum Genet 88: 788–795.
26. Montosi G, Donovan A, Totaro A, Garuti C, Pignatti E, et al. (2001) Autosomal-dominant hemochromatosis is associated with a mutation in the ferroportin (SLC11A3) gene. J Clin Invest 108: 619–623.
27. Njajou OT, Vaessen N, Joosse M, Berghuis B, van Dongen JW, et al. (2001) A mutation in SLC11A3 is associated with autosomal dominant hemochromatosis. Nat Genet 28: 213–214.
28. Kurowski MA, Bujnicki JM (2003) GeneSilico protein structure prediction meta-server. Nucleic Acids Res 31: 3305–3307.
29. Sanchez R, Sali A (2000) Comparative protein structure modeling. Introduction and practical examples with modeller. Methods Mol Biol 143: 97–129.
30. Rauch A, Wieczorek D, Graf E, Wieland T, Endele S, et al. (2012) Range of genetic mutations associated with severe non-syndromic sporadic intellectual disability: an exome sequencing study. Lancet 380: 1674–1682.
31. Volwerk JJ, Shashidhar MS, Kuppe A, Griffith OH (1990) Phosphatidylinositol-specific phospholipase C from Bacillus cereus combines intrinsic phosphotransferase and cyclic phosphodiesterase activities: a 31P NMR study. Biochemistry 29: 8056–8062.
32. Ueda Y, Yamaguchi R, Ikawa M, Okabe M, Morii E, et al. (2007) PGAP1 knock-out mice show otocephaly and male infertility. J Biol Chem 282: 30373–30380.
33. Zoltewicz JS, Plummer NW, Lin MI, Peterson AS (1999) oto is a homeotic locus with a role in anteroposterior development that is partially redundant with Lim1. Development 126: 5085–5095.
34. Zoltewicz JS, Ashique AM, Choe Y, Lee G, Taylor S, et al. (2009) Wnt signaling is regulated by endoplasmic reticulum retention. PLoS One 4: e6191.
35. McKean DM, Niswander L (2012) Defects in GPI biosynthesis perturb Cripto signaling during forebrain development in two new mouse models of holoprosencephaly. Biol Open 1: 874–883.
36. Seelow D, Schuelke M, Hildebrandt F, Nurnberg P (2009) HomozygosityMapper–an interactive approach to homozygosity mapping. Nucleic Acids Res 37: W593–599.
37. McKenna A, Hanna M, Banks E, Sivachenko A, Cibulskis K, et al. (2010) The Genome Analysis Toolkit: a MapReduce framework for analyzing next-generation DNA sequencing data. Genome Res 20: 1297–1303.
38. Li H, Handsaker B, Wysoker A, Fennell T, Ruan J, et al. (2009) The Sequence Alignment/Map format and SAMtools. Bioinformatics 25: 2078–2079.
39. Wang K, Li M, Hakonarson H (2010) ANNOVAR: functional annotation of genetic variants from high-throughput sequencing data. Nucleic Acids Res 38: e164.
40. Abecasis GR, Altshuler D, Auton A, Brooks LD, Durbin RM, et al. (2010) A map of human genome variation from population-scale sequencing. Nature 467: 1061–1073.

Neurogenetics (2014) 15:193–200
DOI 10.1007/s10048-014-0408-y

ORIGINAL ARTICLE

Novel compound heterozygous *PIGT* mutations caused multiple congenital anomalies-hypotonia-seizures syndrome 3

Mitsuko Nakashima · Hirofumi Kashii · Yoshiko Murakami · Mitsuhiro Kato · Yoshinori Tsurusaki · Noriko Miyake · Masaya Kubota · Taroh Kinoshita · Hirotomo Saitsu · Naomichi Matsumoto

Received: 21 February 2014 / Accepted: 25 May 2014 / Published online: 8 June 2014

Abstract Recessive mutations in genes of the glycosylphosphatidylinositol (GPI)-anchor synthesis pathway have been demonstrated as causative of GPI deficiency disorders associated with intellectual disability, seizures, and diverse congenital anomalies. We performed whole exome sequencing in a patient with progressive encephalopathies and multiple dysmorphism with hypophosphatasia and identified novel compound heterozygous mutations, c.250G>T (p. Glu84*) and c.1342C>T (p. Arg488Trp), in *PIGT* encoding a subunit of the GPI transamidase complex. The surface expression of GPI-anchored proteins (GPI-APs) on patient granulocytes was lower than that of healthy controls. Transfection of the Arg488Trp mutant *PIGT* construct, but not the Glu84* mutant, into PIGT-deficient cells partially restored the expression of GPI-APs DAF and CD59. These results indicate that *PIGT* mutations caused neurological impairment and multiple congenital anomalies in this patient.

M. Nakashima · Y. Tsurusaki · N. Miyake · H. Saitsu · N. Matsumoto (✉)
Department of Human Genetics, Yokohama City University Graduate School of Medicine, 3-9 Fukuura, Kanazawa-ku, Yokohama 236-0004, Japan
e-mail: naomat@yokohama-cu.ac.jp

H. Kashii · M. Kubota
Division of Neurology, National Center for Child Health and Development, Tokyo, Japan

Y. Murakami · T. Kinoshita
Research Institute for Microbial Diseases and World Premier International Immunology Frontier Research Center, Osaka University, Osaka, Japan

M. Kato
Department of Pediatrics, Yamagata University Faculty of Medicine, Yamagata, Japan

Keywords Whole exome sequencing · *PIGT* · Compound heterozygous mutations · Glycosylphosphatidylinositol-anchored protein · Multiple congenital anomalies-hypotonia-seizures syndrome 3 · Hypophosphatasia

Introduction

Glycosylphosphatidylinositol (GPI) acts as the anchor of various eukaryotic proteins expressed on the plasma membrane. GPI synthesis and GPI-anchored protein (GPI-AP) modification are mediated by at least 27 genes in the endoplasmic reticulum (ER) and Golgi apparatus [1]. Recent studies have indicated that inherited loss-of-function mutations in these genes lead to GPI deficiencies associated with neurological impairments including seizures, intellectual disability, and multiple congenital anomalies [2–9]. In addition, somatic mutations in PIGA cause paroxysmal nocturnal haemoglobinuria, a haematopoietic disease, which is also caused by somatic mutation of PIGT in combination with the germ line mutation of one allele [10, 11].

PIGT is one of the subunits of the GPI transamidase complex, and catalyzes the attachment of GPI anchors to proteins in the ER [1]. Kvarnung et al. [12] previously reported a homozygous *PIGT* mutation in patients from a consanguineous Turkish family with multiple congenital anomalies-hypotonia-seizures syndrome-3 (MCAHS3 [MIM 615398]). In the present study, we describe the use of whole exome sequencing to identify novel compound heterozygous *PIGT* mutations in a Japanese patient with seizures, intellectual disability and multiple congenital anomalies. Functional analysis indicated that these mutations are causative of GPI deficiency.

Patient and methods

Patient

The female proband was born at full term without asphyxia as the first child of healthy unrelated parents (Fig. 1a). Polyhydramnios was recognized during pregnancy. She showed poor sucking and post-feed stridor soon after birth. At 4 months of age, she showed tonic seizures with apnea and myoclonic seizures, both of which repeatedly turned to convulsive status. Her electroencephalogram (EEG) demonstrated high-amplitude slow wave as a background activity, but no epileptic discharges were observed. She also showed a poor response, muscle hypotonia, unstable head control, a cardiac murmur caused by patent ductus arteriosus, and left hydronephroureter with ureteral stenosis. Her seizures were refractory to multiple antiepileptic drugs such as carbamazepine, clobazam, and an intravenous injection of pyridoxal phosphate while the frequency of her seizures decreased with the combination of valproic acid, zonisamide, and phenytoin to some extent. Phenobarbital could not be used in infancy because of drug eruption. After 1 year of age, she was frequently admitted to hospital because of convulsive status epilepticus induced by fever, or recurrent episodes of respiratory infections, bronchial asthma, or gastroenteritis. Her sleep cycle was disorganized. Brain magnetic resonance imaging at 3 years of age demonstrated progressive atrophy of the cerebral hemisphere, cerebellum, and brainstem (Fig. 1c). EEG at 3 years showed borderline findings consisting of a predominance of fast wave activity with no spindle formation interrupted by slow wave burst. She recurrently suffered bone fractures without obvious event. Systemic bone X-ray at 12 years of age showed neurogenic arthrogryposis and osteoporosis. At 12 years of age, she was bedridden and was only able to roll over. She showed profound intellectual disability and had no meaningful words. Her epileptic seizures disappeared after 10 years of age, but epileptic discharges comprised of spike-and-slow wave complex at bilateral frontal area with low-amplitude irregular background activity were seen on EEG.

G-banded chromosomal analysis revealed a normal karyotype (46,XX). Metabolic screenings including amino acids, lactic acid, pyruvic acid, organic acids, lactic acid, and lysosomal enzymes were unremarkable. The biochemical analysis of blood repeatedly showed low levels of serum alkaline phosphatase from birth (186 U/l at birth and 326 U/l at 7 years of age [normal range, 450–1250 U/l]). Both concentrations of serum and urine calcium were normal (serum calcium, 9.6 mg/dl; U-calcium/U-creatinine ratio, 0.23 at 7 years of age).

DNA preparation

Peripheral blood samples were obtained from the patient and her parents after parents signed informed consent. DNA was extracted using QuickGene-610 L (Fujifilm, Tokyo, Japan) according to the manufacturer's instructions. The study was approved by the ethics committee of the Yokohama City University.

Whole exome sequencing

Patient DNA was captured with the SureSelect Human All Exon V5 Kit (Agilent Technologies, Santa Clara, CA, USA) and sequenced on an Illumina Hiseq2000 (Illumina, San Diego, CA, USA) with 101-bp paired-end reads. Image analysis and base calling were performed by sequence control software real-time analysis and CASAVA software v1.8 (Illumina). Reads were mapped to the human reference genome sequence (UCSC hg19, NCBI build 37) and aligned using Novoalign (Novocraft Technologies, Jaya, Malaysia). PCR duplicate reads were excluded using Picard (http://picard.sourceforge.net/) for further analysis. Single-nucleotide variants (SNVs) and small indels were identified using the Genome Analysis Toolkit UnifiedGenotyper [13] and filtered according to the Broad Institute's best-practice guidelines (version 3). Variants that passed the filters were annotated using ANNOVAR[14]. The damaging prediction was performed by Polyphen-2 [15] and MutationTaster software [16].

Sanger sequencing

PIGT exon 2 and exon 10 sequences were PCR amplified from the patient and her parents using the following primers: *PIGT* ex2F 5′-GGGAGGAACTTGTCATCACC-3′ and ex2R 5′-CAGTGGCAGGATGACAACAC-3′, *PIGT* ex10F 5′-AGAGATGTGGGTGACCTTGC-3′ and ex10R 5′-CTGAGGACAGATGGGCTACA-3′, respectively. Amplified PCR products were sequenced on an ABI 3500xl or 3130xl Genetic Analyzer (Applied Biosystems, Foster City, CA, USA).

Flow cytometry

Peripheral blood samples were collected from the patient and normal control individuals. Granulocyte surface expression of total GPI-APs was quantified by staining with Alexa 488-conjugated inactivated aerolysin (FLAER; Protox Biotech, Victoria, Canada). Expression of CD16, CD24, and alkaline phosphatase (ALP) was examined using appropriate primary antibodies (3G8, ML5, and B4-78, respectively; BD Biosciences, Franklin Lakes, NJ, USA), followed by a PE-conjugated anti-mouse IgG secondary antibody (BD Biosciences). Cells were analyzed by BD FACSCanto II (BD Biosciences).

Human *PIGT* cDNA (NM_015937.5) with FLAG at the C terminus was subcloned into the pME (driven by a strong SRα promoter) or pTA (driven by a weak promoter

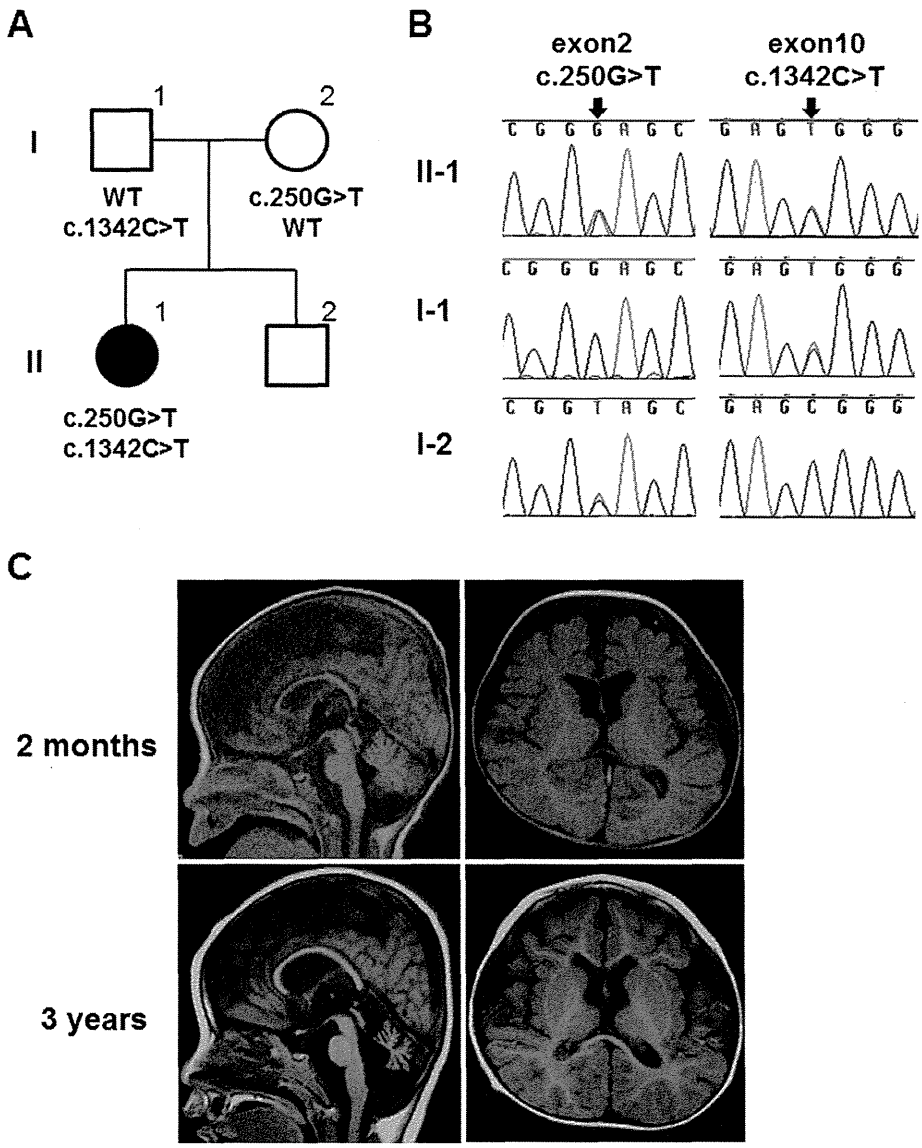

Fig. 1 **a** Familial pedigree. **b** Sanger sequencing results. Compound heterozygous mutations, c.250G>T and c.1342C>T, in *PIGT* were observed in the affected individual. c.250G>T (*left*) and c.1342C>T (*right*) were inherited from the mother and the father, respectively. **c** Magnetic resonance imaging of the patient's brain. Axial and sagittal T1-weighted images at 3 years of age show atrophic changes of the cerebral hemisphere, brainstem, and cerebellum

containing only TATA-box) vector [17]. Two *PIGT* mutants, Glu84* and Arg488Trp, were generated by site-directed mutagenesis. Mutant and wild-type *PIGT* plasmids were transfected by electroporation into CHO H4, *PIGT*-deficient Chinese hamster ovary (CHO) cells expressing human DAF (also called CD55) and CD59 as previously described [18]. Two days later, lysates were run on SDS-PAGE, and Western blotting was performed using an anti-FLAG antibody (M2; Sigma-Aldrich, St. Louis, MO, USA) to detect FLAG-tagged PIGT (PIGT-F). The protein levels were normalized to the loading control, and luciferase activities were used to evaluate transfection efficiencies. Cells were stained with anti-hCD59 (5H8), anti-hDAF (IA10), and anti-Hamster uPAR (5D6) antibodies and restoration of the surface expression of GPI-APs was assessed by flow cytometry.

Results

Mutation screening

We performed mutation screening for previously reported genes involved in the GPI-anchor–synthesis pathway, and identified the compound heterozygous mutations c.250G>T (p. Glu84*) and c.1342C>T (p. Arg488Trp) in *PIGT* (NM_015937.5). Both mutations were not found in 6500

ESP (Exome Sequencing Project) or 1000 genomes [19, 20], but c.1342C>T is present in one of 408 in-house control exomes. Both mutations were predicted to be probably disease-causing by Polyphen-2 and MutationTaster. Sanger sequencing confirmed that c.250G>T and c.1342C>T were inherited from the mother and father, respectively (Fig. 1b).

Functional effect of the mutations on GPI synthesis

PIGT is a component of GPI transamidase that mediates the post-translational attachment of GPI anchors to the C-terminal of the precursor protein. Therefore, the mutant GPI transamidase is likely to impair the surface expression of GPI-APs. To investigate the influence of *PIGT* mutations on GPI-APs synthesis, we first examined the granulocyte surface expression of GPI-APs from the patient and a healthy control. Expression of total GPI-APs (FLAER staining) and GPI-APs CD16 and ALP on granulocytes was reduced in the patient compared to the normal control (Fig. 2a). However, similar expression levels of another GPI-AP CD24 were seen in the patient and control (Fig. 2a).

We then transiently transfected wild-type or mutant (Glu84* or Arg488Trp) *PIGT* cDNA constructs into *PIGT*-deficient CHO cells to evaluate the functional effect of each mutation on GPI-AP expression. Western blotting revealed that the expression level of Arg488Trp mutant protein was similar to that of wild-type protein, whereas the Glu84* mutant expressed a small amount of full-length protein (probably read-though) (Fig. 2c). Wild-type *PIGT* transfection successfully restored the expression of GPI-APs CD59, DAF (CD55), and uPAR in both cases using vectors with a strong (pME) and weak (pTA) promoter (Fig. 2b). The Arg488Trp mutant *PIGT* cloned in pME restored the expression of GPI-APs close to that of wild-type, whereas the same mutant in the pTA vector only partially restored expression. The Glu84* mutant *PIGT* in the pME vector insufficiently restored the expression of GPI-APs, while this mutant in the pTA vector could not restore expression (Fig. 2b). These results demonstrate that both mutants, especially the Glu84* alteration, reduce the activity of PIGT function.

Fig. 2 **a** Surface expression of GPI-APs on granulocytes. Granulocytes from the patient and healthy control were stained with FLAER or antibodies against CD24, CD16, and ALP. The expression of total GPI, CD16, and ALP in the patient (*solid line*) was lower than in the normal control (*dark shaded area*). CD24 expression did not differ between the patient and control. The *light shaded areas* represent the isotype control. *X* axes show fluorescent intensities, which indicate expression levels of each GPI-AP on the cell surface. *Y* axes show the relative cell numbers. The value of mean fluorescent intensities of each sample is shown in each panel. **b** PIGT-deficient CHO cells were transiently transfected with wild-type (*dashed line*), Glu84* mutant (*fine solid line*), or Arg488Trp mutant (*bold solid line*) *PIGT* cDNA expression constructs in vectors with either a strong promoter (pME; *upper panels*) or weak promoter (pTA; *lower panels*). PIGT-F protein levels and restoration of the surface expression of CD59, DAF, and uPAR were assessed 2 days later. The *dark* and *light shadows* represent empty-vector transfectants and isotype controls, respectively. **c** Western blotting showed that the Arg488Trp mutant protein was expressed at similar levels to the wild-type protein, whereas the Glu84* mutant full-length protein, representing the read-through product, was expressed at lower levels. Quantity numbers at the bottom of the gel indicate the relative intensity of PIGT-F protein levels normalized to the loading control, and luciferase activities used for evaluating transfection efficiencies. *Arrowhead* indicates a non-specific product

Discussion

GPI deficiency syndromes are recessive disorders caused by mutations in genes involved in the GPI-anchor biosynthesis pathway. Here, we describe novel compound heterozygous *PIGT* mutations in a nonconsanguineous patient presenting with seizures and intellectual disability.

The first reported *PIGT* mutation (c.547A>C, p.Thr183Pro) was identified in a consanguineous Turkish family who showed seizures, intellectual disability, and multiple congenital anomalies [12]. A decreased expression of GPI-APs was documented on patient granulocytes. They confirmed that the homozygous c.547A>C mutation impaired the function of PIGT by the functional study using *pigt* knockdown zebrafish embryos which showed gastrulation defects phenotype. In the present study, we also demonstrated that both *PIGT* mutations, c.250G>T (p. Glu84*) and c.1342C>T (p. Arg488Trp), impaired the function of PIGT which was confirmed by the functional study using the PIGT deficient CHO cells.

Mammalian GPI transamidase consists of at least five subunits, PIGK, GPAA1, PIGS, PIGT, and PIGU [1]. Of these, PIGT plays a critical role in stabilizing the complex formation of GPI transamidase [17], which mediates cleavage of the GPI attachment signal peptide at the C-terminal of the precursor protein and transfers GPI anchors to the C-terminal of cleaved proteins [1]. Consequently, PIGT mutants may not be able to correctly form the GPI transamidase complex, leading to a loss of GPI transamidase activity and reduction in the cellular surface expression of GPI-APs.

Our patient and four patients described by Kvarnung et al. [12] showed broad clinical spectrum and shared several common features (Table 1). The neurological findings including intractable seizures, hypotonia and severe intellectual disability were observed in all patients. Ophthalmologic features including strabismus, nystagmus, and cerebral visual impairment were also observed in all. Cerebral and cerebellar atrophy was observed in our patient and two of four seen by Kvarnung et al. The EEG findings in our patient were also exacerbated as she grew, suggesting progressive encephalopathy. Our patient and three of four patients by Kvarnung et al. had some cardiologic disorders. All patients had some

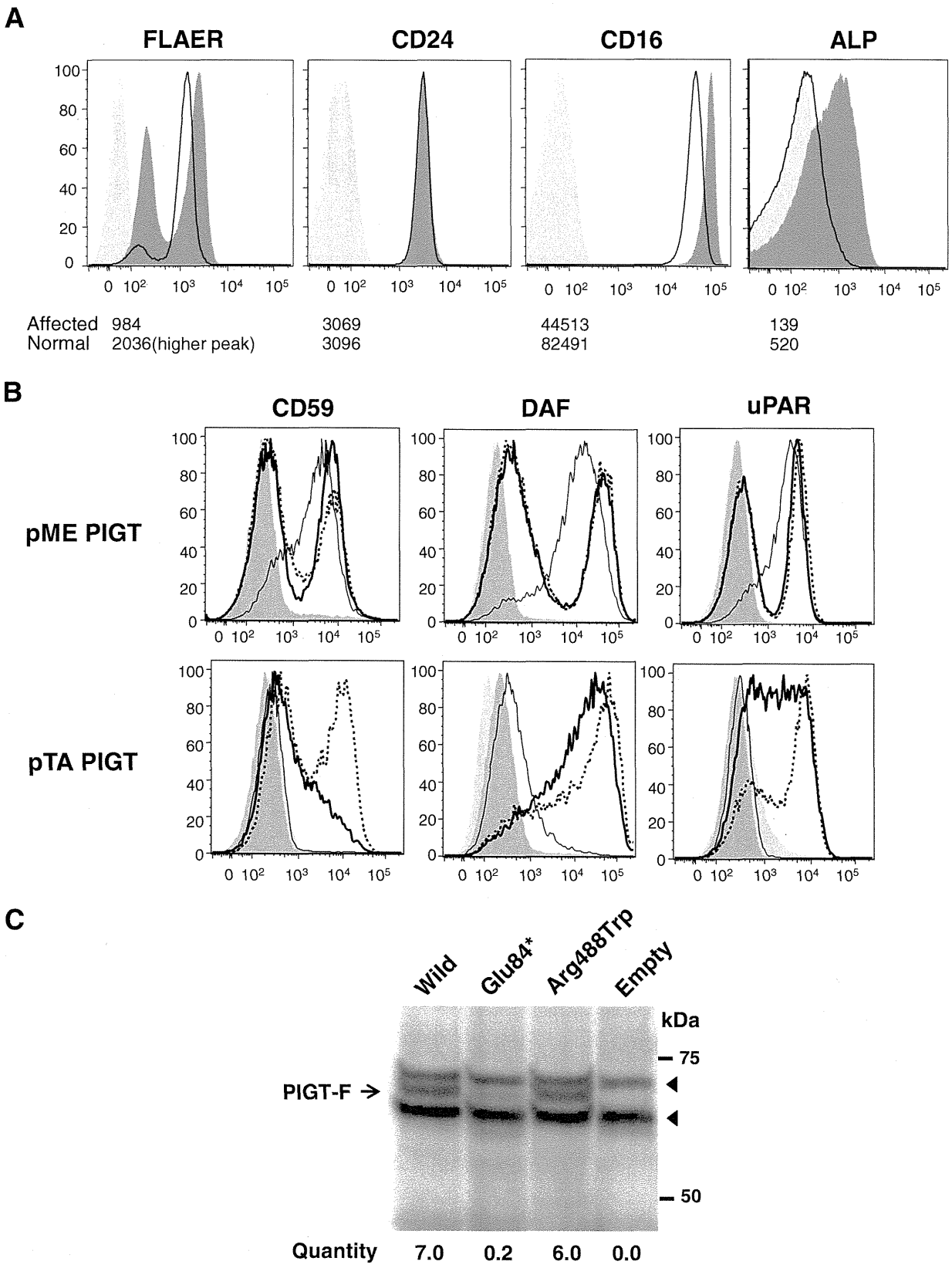
A
FLAER
CD24
CD16
ALP
Affected 984 3069 44513 139
Normal 2036(higher peak) 3096 82491 520
B
CD59
DAF
uPAR
pME PIGT
pTA PIGT
C
Wild
Glu84*
Arg488Trp
Empty
kDa
75
50
PIGT-F
Quantity 7.0 0.2 6.0 0.0

Table 1 Clinical features of patients with PIGT mutations

Patients	This Patient	Kvarnung et al. Patient 1	Kvarnung et al. Patient 2	Kvarnung et al. Patient 3	Kvarnung et al. Patient 4
consanguinity	–	+	+	+	+
Sex	Female	Female	Female	Female	Female
Gestation	40 weeks	40 weeks	39 weeks	37 weeks	37 weeks
Birth weight	3,816 g	4,735 g	4,500 g	3,460 g	3,240 g
Birth length	51 cm	53 cm	54 cm	53 cm	53 cm
BHC	35.5 cm +1.8 SD	38 cm +2 SD	39 cm +3 SD	35 cm +1 SD	36 cm +1.5 SD
HPP	+	+	+	+	+
ID	+	+	+	+	+
Hypotonia	+	+	+	+	+
Seizure	+	+	+	+	+
Strabismus	+	+	+	+	+
Nystagmus	+	+	+	+	+
CVI	+	+	+	+	+
Brain images	CT: dilated ventricle, frontal atrophy, cerebellar and brainstem atrophy	CT: primitive Sylvian fissures	CT: Normal findings	MRI: global atrophy with predominate vermis and cerebellar atrophy, atrophy of basal ganglia	MRI: global atrophy with predominat vermis and cerebellar atrophy, hypomyelination
Tooth abnormalities	–	+	+	+	+
Skeletal features	Scoliosis, osteoporosis	Craniosynostosis, Pectus excavatum, Short arm, Scoliosis, Delayed bone age, Reduced mineralisation	Craniosynostosis, short arm, Scoliosis, Delayed bone age, Reduced mineralisation	Short arm, Delayed bone age, Reduced mineralisation	Short arm, Delayed bone age, Reduced mineralisation
Urologic features	Urolithiasis, Ureteral dilation	Nephrocalcinosis	Nephrocalcinosis, Ureteral dilation, Cysts and dysplasia	Nephrocalcinosis, Ureteral dilation	Nephrocalcinosis, Ureteral dilation
Cardiologic features	PDA	Minor PDA	–	Mild restrictive CMP	Increased atrial load on ECG
Facial features	Low set ears, micrognathia, malar flattening, upslanting palpebral fissures, depressed nasal bridge, short anteverted nose, downturned corners of the mouth, tented lip, high arched palate	High forehead with bitemporal narrowing, broad nasal root, anteverted nose, long philtrum with a deep groove, distinct cupid bow	High forehead with bitemporal narrowing, broad nasal root, anteverted nose, long philtrum with a deep groove, distinct cupid bow	High forehead with bitemporal narrowing, broad nasal root, anteverted nose, long philtrum with a deep groove, distinct cupid bow	High forehead with bitemporal narrowing, broad nasal root, anteverted nose, long philtrum with a deep groove, distinct cupid bow

BHC birth head circumference, *HPP* hypophosphatasia, *ID* intellectual disability, *CVI* cerebral visual impairment, *ECG* electrocardiogram, *CMP* cardiomyopathy, *PDA* patent ductus arteriosus

urologic features, but not nephrocalcinosis in our patient. Our case shared similar facial features with previous patients including a depressed nasal bridge, short anteverted nose, tented lip, and downturned corners of the mouth. Low set ears, micrognathia, malar flattening, and upslanting palpebral fissures were unique to our patient.

Hyperphosphatasia is a characteristic symptom of some GPI deficiencies, such as PIGV, PIGW, PIGO, PGAP2 and PGAP3 deficiencies [2–6]. In contrast, hypophosphatasia is a particularly distinctive feature in the loss of GPI transamidase function. Murakami at al. suggested that GPI transamidase abnormalities lead to an inability to hydrolyze the precursor protein of alkaline phosphatase, resulting in the degradation of most precursor proteins within the cell and a decrease of serum alkaline phosphatase levels (hypophosphatasia) [21]. This is supported in our case by the hypophosphatasia. The patients described by Kvarnung et al. showed hypercalcemia and hypercalciuria following tooth abnormality, craniosynostosis, a delayed bone age, and reduced mineralization, which is the common features with infantile hypophosphatasia caused by the mutations in *ALPL*, the gene encoding tissue non-specific alkaline phosphatase (TNAP) [22]. As TNAP is a GPI-AP, the PIGT deficiency causes decreased surface expression of TNAP, which would lead to bone abnormalities. Regardless of hypophosphatasia, our case showed only mild scoliosis and osteoporosis, but no tooth abnormality nor craniosynostosis. Different mutational effects on the enzyme activity may account for such different phenotypes. In this study, mutant PIGT construct harboring Arg488Trp or Glu84* in strong promoter (pME) vector restored GPI-Aps expression. In contrast, Kvarnung et al. showed that abnormal phenotype of pigt knockdown zebrafish was never restored by the homozygous mutant (Thr183Pro) PIGT cDNA. Therefore, it is possible to estimate that the Thr183Pro mutation may affect the GPI transamidase complex activity more severely than the Arg488Trp and Glu84* mutations, leading to less severe phenotypes. However, further functional analysis and cases with *PIGT* mutations are needed to elucidate the relevance of these mutations in PIGT function and full clinical spectrum of GPI deficiency syndromes.

Acknowledgments We thank the patient's family for participating in this work. We also thank Nobuko Watanabe for her technical assistance. This study was supported by the Ministry of Health, Labour and Welfare of Japan, a Grant-in-Aid for Scientific Research (A), (B), and (C) from the Japan Society for the Promotion of Science, the Takeda Science Foundation, the fund for Creation of Innovation Centers for Advanced Interdisciplinary Research Areas Program in the Project for Developing Innovation Systems, the Strategic Research Program for Brain Sciences, and a Grant-in-Aid for Scientific Research on Innovative Areas (Transcription Cycle) from the Ministry of Education, Culture, Sports, Science and Technology of Japan.

Conflict of interest The authors declare that they have no conflict of interest.

References

1. Kinoshita T, Fujita M, Maeda Y (2008) Biosynthesis, remodelling and functions of mammalian GPI-anchored proteins: recent progress. J Biochem 144(3):287–294. doi:10.1093/jb/mvn090
2. Krawitz PM, Schweiger MR, Rodelsperger C, Marcelis C, Kolsch U, Meisel C, Stephani F, Kinoshita T, Murakami Y, Bauer S, Isau M, Fischer A, Dahl A, Kerick M, Hecht J, Kohler S, Jager M, Grunhagen J, de Condor BJ, Doelken S, Brunner HG, Meinecke P, Passarge E, Thompson MD, Cole DE, Horn D, Roscioli T, Mundlos S, Robinson PN (2010) Identity-by-descent filtering of exome sequence data identifies PIGV mutations in hyperphosphatasia mental retardation syndrome. Nat Genet 42(10):827–829. doi:10.1038/ng.653
3. Krawitz PM, Murakami Y, Hecht J, Kruger U, Holder SE, Mortier GR, Delle Chiaie B, De Baere E, Thompson MD, Roscioli T, Kielbasa S, Kinoshita T, Mundlos S, Robinson PN, Horn D (2012) Mutations in PIGO, a member of the GPI-anchor-synthesis pathway, cause hyperphosphatasia with mental retardation. Am J Hum Genet 91(1):146–151. doi:10.1016/j.ajhg.2012.05.004
4. Hansen L, Tawamie H, Murakami Y, Mang Y, ur Rehman S, Buchert R, Schaffer S, Muhammad S, Bak M, Nothen MM, Bennett EP, Maeda Y, Aigner M, Reis A, Kinoshita T, Tommerup N, Baig SM, Abou Jamra R (2013) Hypomorphic mutations in PGAP2, encoding a GPI-anchor-remodeling protein, cause autosomal-recessive intellectual disability. Am J Hum Genet 92(4):575–583. doi:10.1016/j.ajhg.2013.03.008
5. Howard MF, Murakami Y, Pagnamenta AT, Daumer-Haas C, Fischer B, Hecht J, Keays DA, Knight SJ, Kolsch U, Kruger U, Leiz S, Maeda Y, Mitchell D, Mundlos S, Phillips JA 3rd, Robinson PN, Kini U, Taylor JC, Horn D, Kinoshita T, Krawitz PM (2014) Mutations in PGAP3 impair GPI-anchor maturation, causing a subtype of hyperphosphatasia with mental retardation. Am J Hum Genet 94(2):278–287. doi:10.1016/j.ajhg.2013.12.012
6. Chiyonobu T, Inoue N, Morimoto M, Kinoshita T, Murakami Y (2013) Glycosylphosphatidylinositol (GPI) anchor deficiency caused by mutations in PIGW is associated with West syndrome and hyperphosphatasia with mental retardation syndrome. J Med Genet. doi:10.1136/jmedgenet-2013-102156
7. Krawitz PM, Murakami Y, Riess A, Hietala M, Kruger U, Zhu N, Kinoshita T, Mundlos S, Hecht J, Robinson PN, Horn D (2013) PGAP2 mutations, affecting the GPI-anchor-synthesis pathway, cause hyperphosphatasia with mental retardation syndrome. Am J Hum Genet 92(4):584–589. doi:10.1016/j.ajhg.2013.03.011
8. Almeida AM, Murakami Y, Layton DM, Hillmen P, Sellick GS, Maeda Y, Richards S, Patterson S, Kotsianidis I, Mollica L, Crawford DH, Baker A, Ferguson M, Roberts I, Houlston R, Kinoshita T, Karadimitris A (2006) Hypomorphic promoter mutation in PIGM causes inherited glycosylphosphatidylinositol deficiency. Nat Med 12(7):846–851. doi:10.1038/nm1410
9. Ng BG, Hackmann K, Jones MA, Eroshkin AM, He P, Wiliams R, Bhide S, Cantagrel V, Gleeson JG, Paller AS, Schnur RE, Tinschert S, Zunich J, Hegde MR, Freeze HH (2012) Mutations in the glycosylphosphatidylinositol gene PIGL cause CHIME syndrome. Am J Hum Genet 90(4):685–688. doi:10.1016/j.ajhg.2012.02.010
10. Johnston JJ, Gropman AL, Sapp JC, Teer JK, Martin JM, Liu CF, Yuan X, Ye Z, Cheng L, Brodsky RA, Biesecker LG (2012) The phenotype of a germline mutation in PIGA: the gene somatically mutated in paroxysmal nocturnal hemoglobinuria. Am J Hum Genet 90(2):295–300. doi:10.1016/j.ajhg.2011.11.031
11. Krawitz PM, Hochsmann B, Murakami Y, Teubner B, Kruger U, Klopocki E, Neitzel H, Hoellein A, Schneider C, Parkhomchuk D, Hecht J, Robinson PN, Mundlos S, Kinoshita T, Schrezenmeier H (2013) A case of paroxysmal nocturnal hemoglobinuria caused by a

germline mutation and a somatic mutation in PIGT. Blood 122(7): 1312–1315. doi:10.1182/blood-2013-01-481499
12. Kvarnung M, Nilsson D, Lindstrand A, Korenke GC, Chiang SC, Blennow E, Bergmann M, Stodberg T, Makitie O, Anderlid BM, Bryceson YT, Nordenskjold M, Nordgren A (2013) A novel intellectual disability syndrome caused by GPI anchor deficiency due to homozygous mutations in PIGT. J Med Genet 50(8):521–528. doi: 10.1136/jmedgenet-2013-101654
13. DePristo MA, Banks E, Poplin R, Garimella KV, Maguire JR, Hartl C, Philippakis AA, del Angel G, Rivas MA, Hanna M, McKenna A, Fennell TJ, Kernytsky AM, Sivachenko AY, Cibulskis K, Gabriel SB, Altshuler D, Daly MJ (2011) A framework for variation discovery and genotyping using next-generation DNA sequencing data. Nat Genet 43(5):491–498. doi:10.1038/ng.806
14. Wang K, Li M, Hakonarson H (2010) ANNOVAR: functional annotation of genetic variants from high-throughput sequencing data. Nucleic Acids Res 38(16):e164. doi:10.1093/nar/gkq603
15. Adzhubei IA, Schmidt S, Peshkin L, Ramensky VE, Gerasimova A, Bork P, Kondrashov AS, Sunyaev SR (2010) A method and server for predicting damaging missense mutations. Nat Methods 7(4):248–249. doi:10.1038/nmeth0410-248
16. Schwarz JM, Rodelsperger C, Schuelke M, Seelow D (2010) MutationTaster evaluates disease-causing potential of sequence alterations. Nat Methods 7(8):575–576. doi:10.1038/nmeth0810-575
17. Ohishi K, Inoue N, Kinoshita T (2001) PIG-S and PIG-T, essential for GPI anchor attachment to proteins, form a complex with GAA1 and GPI8. EMBO J 20(15):4088–4098. doi:10.1093/emboj/20.15.4088
18. Ashida H, Hong Y, Murakami Y, Shishioh N, Sugimoto N, Kim YU, Maeda Y, Kinoshita T (2005) Mammalian PIG-X and yeast Pbn1p are the essential components of glycosylphosphatidylinositol-mannosyltransferase I. Mol Biol Cell 16(3):1439–1448. doi:10.1091/mbc.E04-09-0802
19. Genomes Project C, Abecasis GR, Altshuler D, Auton A, Brooks LD, Durbin RM, Gibbs RA, Hurles ME, McVean GA (2010) A map of human genome variation from population-scale sequencing. Nature 467(7319):1061–1073. doi:10.1038/nature09534
20. Genomes Project C, Abecasis GR, Auton A, Brooks LD, DePristo MA, Durbin RM, Handsaker RE, Kang HM, Marth GT, McVean GA (2012) An integrated map of genetic variation from 1,092 human genomes. Nature 491(7422):56–65. doi:10.1038/nature11632
21. Murakami Y, Kanzawa N, Saito K, Krawitz PM, Mundlos S, Robinson PN, Karadimitris A, Maeda Y, Kinoshita T (2012) Mechanism for release of alkaline phosphatase caused by glycosylphosphatidylinositol deficiency in patients with hyperphosphatasia mental retardation syndrome. J Biol Chem 287(9):6318–6325. doi:10.1074/jbc.M111.331090
22. Mornet E (2007) Hypophosphatasia. Orphanet J Rare Dis 2:40. doi: 10.1186/1750-1172-2-40

EUROPEAN JOURNAL OF Haematology

European Journal of Haematology 92 (450–453)

CASE REPORT

Paroxysmal nocturnal hemoglobinuria with copy number-neutral 6pLOH in GPI (+) but not in GPI (−) granulocytes

Yasutaka Ueda[1], Jun-ichi Nishimura[2], Yoshiko Murakami[3,4], Sachiko Kajigaya[1], Taroh Kinoshita[3,4], Yuzuru Kanakura[2], Neal S. Young[1]

[1]Hematology Branch, National Heart, Lung, and Blood Institute, National Institutes of Health, Bethesda, MD, USA; [2]Department of Hematology and Oncology, Osaka University Graduate School of Medicine, Osaka; [3]Department of Immunoregulation, Research Institute for Microbial Diseases, Osaka University, Osaka; [4]Department of Immunoglycobiology, WPI Immunology Frontier Research Centre, Osaka University, Osaka, Japan

Abstract

Paroxysmal nocturnal hemoglobinuria (PNH) is an acquired bone marrow disorder caused by expansion of a clone of hematopoietic cells lacking glycosylphosphatidylinositol (GPI)-anchored membrane proteins. Multiple lines of evidence suggest immune attack on normal hematopoietic stem cells provides a selective growth advantage to PNH clones. Recently, frequent loss of HLA alleles associated with copy number-neutral loss of heterozygosity in chromosome 6p (CN-6pLOH) in aplastic anemia (AA) patients was reported, suggesting that AA hematopoiesis 'escaped' from immune attack by loss of HLA alleles. We report here the first case of CN-6pLOH in a Japanese PNH patient only in GPI-anchored protein positive (59%) granulocytes, but not in GPI-anchored protein negative (41%) granulocytes. CN-6pLOH resulted in loss of the alleles *A*02:06-DRB1*15:01-DQB1*06:02*, which have been reported to be dominant in Japanese PNH patients. Our patient had maintained nearly normal blood count for several years. Our case supports the hypothesis that a hostile immune environment drives selection of resistant hematopoietic cell clones and indicates that clonal evolution may occur also in normal phenotype (non-PNH) cells in some cases.

Key words paroxysmal nocturnal hemoglobinuria; array comparative genomic hybridization; loss of heterozygosity; clonal evolution; bone marrow failure syndromes

Correspondence Yasutaka Ueda, Hematology Branch, NHLBI/NIH, Bldg 10-CRC, Rm 3E-5216, 9000 Rockville Pike, Bethesda, MD 20892, USA. Tel: 301-451-7132; Fax: 301-496-8396; e-mail: ueday2@nhlbi.nih.gov

Accepted for publication 15 December 2013 doi:10.1111/ejh.12253

Paroxysmal nocturnal hemoglobinuria (PNH) is a rare, life-threatening bone marrow failure syndrome, which is characterized by three major features: intravascular hemolytic anemia, bone marrow failure, and thrombosis (1). PNH is an acquired clonal disorder of the hematopoietic stem cell (HSC) caused by a somatic mutation of the X-linked phosphatidylinositol glycan class A (*PIGA*) gene in one or a few hematopoietic stem cells (2). Even healthy individuals were reported to have very small number of PNH cells (3). The mechanism of clonal expansion of PNH cells is not understood, but the close association between PNH and aplastic anemia (AA) suggests that immune-mediated attack to hematopoietic stem cells underlies the pathogenesis of the association. Some data support a model of PNH clone expansion based on autoimmunity. PNH clones were less sensitive to NK and T-cell killing due to lack of expression of stress-inducible GPI-anchored proteins ULBP1 and ULBP2 in vitro and with patients granulocytes (4, 5), and an inefficient T lymphocyte response was observed to GPI (−) cells *in vitro* and in mouse models (6). Recently, frequent loss of HLA alleles associated with copy number-neutral loss of heterozygosity of the 6p arms (CN-6pLOH) in AA patients was reported (7). Here, we describe the first case of a PNH patient with CN-6pLOH in GPI (+) granulocytes, but not in GPI (−) granulocytes.

Patient and methods

A 33-year-old male presented to hospital for mild thrombocytopenia (130×10^9/L), and PNH was diagnosed by flow

cytometry (1). The patient had not been treated for 2 years and 6 months due to lack of symptoms of anemia or thrombosis, although he had experienced hemoglobinuria several times a year since diagnosis. PNH clone sizes were 49.0% and 22.0% in granulocytes and red blood cells, respectively, at diagnosis and were 45.2% and 28.5%, respectively, 12 months after the diagnosis. LDH had remained elevated (500–600 U/L). At the time of array comparative genomic hybridization (aCGH) analysis, 24 months after the diagnosis, the proportions of GPI-negative cells were 40.9%, 25.7%, and 4.7% in granulocytes, red blood cells, and T cells, respectively. Blood count included leukocytes 3.7×10^9/L, (38.8% neutrophils, 48.0% lymphocytes, 8.7% monocytes, 0.8% eosinophils, and 0.5% basophils), hemoglobin 14.4 g/dL, MCV 101.9 fl, platelets 113×10^9/L, and reticulocyte count 112×10^9/L. LDH was elevated at 620 U/L (normal range up to 229 U/L). Informed consent was obtained from the patient in accordance with protocols approved by the Institutional Review Boards of Osaka University Hospital. Red blood cells were analyzed for GPI-anchored proteins with anti-CD55 and anti-CD59 antibodies within a CD235 positive population. Peripheral blood granulocytes (CD11b + 7AAD−) and T cells (CD3 + 7AAD−) were separated into GPI (+) and GPI (−) cells by Flaer (Pinewood Scientific Services, Victoria, BC, Canada) staining. After sorting, each cell population of granulocytes was subjected to DNA extraction with the QIAamp DNA Blood Mini kit or the QIAamp DNA Micro kit (QIAGEN, Hilden, Germany). High-resolution genome-wide DNA copy number analysis was performed with both GPI (+) and GPI (−) granulocytes using the CytoScan®HD Array (Affymetrix, Santa Clara, CA, USA). Sample processing was performed at Coriell Genotyping and Microarray Center, Coriell Institute for Medical Research (Camden, NJ, USA). Data were analyzed with Affymetrix Chromosome Analysis Suite (CHAS). For the analysis of clonal lesions, loss of heterozygosity (LOH) was called when the deletion was more than 25 Mb and involved telomeres (8). Alleles at *HLA-A*, *-B*, *-DRB1*, *-DQB1*, and *-DPB1* loci were identified by PCR and sequence-specific oligonucleotide probes (PCR-SSOP) method using the WAKFlow HLA Typing kit (Wakunaga, Hiroshima, Japan) at the HLA Foundation Laboratory (Kyoto, Japan), as described previously (9). Briefly, target DNA was PCR amplified with 5′-biotin-labeled primers that are highly specific to sequences of HLA genes. Amplified DNA was denatured and hybridized to locus-specific probes conjugated to microbeads labeled with streptavidin–phycoerythrin. The fluorescent intensity of phycoerythrin on each coded oligobead was measured by the Luminex® 100 system (Luminex, Austin, TX, USA). The data analysis was performed using the WAKFlow® Typing Software (Wakunaga). The haplotypes of six loci were inferred based on the data of haplotype frequencies of a Japanese population (701 families; $n = 2972$) estimated by direct counting method. The data are available at the Web site of the HLA Foundation Laboratory (http://hla.or.jp/haplo/haplonavi.php?type=haplo&lang=en).

Results and discussion

The Affymetrix CytoScan® HD Array contains more than 2.4 million markers for copy numbers and 750 thousand single nucleotide polymorphisms, enabling detection of high-resolution copy number, LOH detection, and breakpoint estimation across the genome. We employed the CytoScan®HD Array for aCGH analysis of submicroscopic aberrations of genomes in three Japanese PNH patients who had both GPI (+) and GPI (−) cells in granulocytes. Remarkably, CN-6pLOH was detected in a GPI (+) granulocyte population, but not in a GPI (−) granulocyte popula-

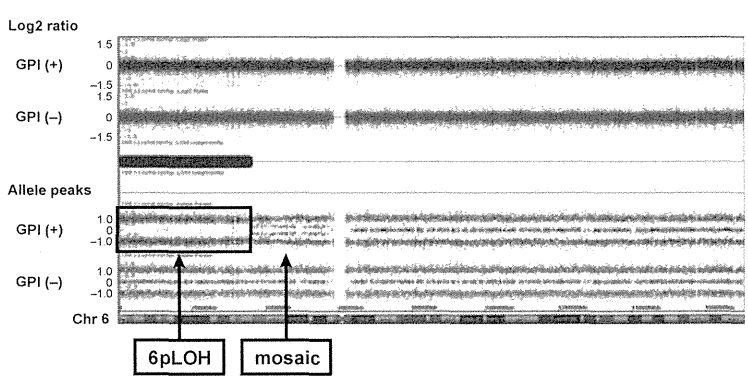

Figure 1 Acquired CN-6pLOH in GPI (+) granulocytes but not in GPI (−) granulocytes. Upper panel shows copy number status by log2 ratio: Theoretically, the log 2 ratio of normal (copy number-neutral) clones is log2 (2/2) = 0 and of single copy losses is log2 (1/2) = −1. Lower panel shows allele frequency calculated as the difference between the signals of the A allele minus B allele. Homozygous AA maps to approximately +1, and homozygous BB allele maps to approximately −1, with the heterozygote mapping to approximately 0. Single A and B allele maps to 0.5 and −0.5, respectively. Copy number was neutral in 6p arm, but loss of heterozygosity (the disappearance of the heterozygote signal) was observed with mosaicism near the centromere.

tion, in a single patient (Fig. 1). Mosaicism was observed near the centromere of 6p, suggesting there were at least two clones with CN-6pLOH in GPI (+) cells. Both of the CN-LOH covered HLA class I and class II genes (6p21.2–6p25.3 and 6p11.2–6p25.3). HLA typing of the patient by PCR-SSOP method was *A*02:06, A*26:02, B*35:01, B*40:06, C*03:03, C*08:01, DRB1*09:01, DRB1*15:01, DQB1*03:03, DQB1*06:02, DPB1*02:01, DPB1*05:01*. The haplotype of *A*02:06-B*35:01-C*03:03-DRB1*15:01-DQB1*06:02- DPB1*05:01* was lost in 80%–90% of GPI (+) granulocytes due to 6pLOH. High frequency of CN-6pLOH in AA patients was reported by a Japanese group (7), and particular alleles including *HLA-A*02:06* were dominantly missing, suggesting 6pLOH hematopoietic stem cells escape from the immune attack mediated by cytotoxic T cells (CTLs), which may recognize unknown antigens on class I HLA molecules. HLA alleles *A*02:06, DRB1*15:01,* and *DQB1*06:02* were reported to be frequent among Japanese PNH patients (10, 11), suggesting that an immunological mechanism underlies the expansion of PNH clones. Immune mechanisms have long been hypothesized for the expansion of PNH clones with some support in the literatures. PNH clones were reported to be less sensitive to NK and T-cell killing (4, 5) or CD4 + T cells (6). GPI itself was suggested to be an autoantigen recognized by GPI-specific T cells (12, 13). GPI (+) granulocytes reflect purportedly 'normal' hematopoiesis, but our previous studies showed frequent chromosomal abnormalities and apoptotic gene expression in this 'normal' population. Based on these observations, in this patient, 80% to 90% of GPI (+) granulocytes were derived from clones that might have escaped immune attack by loss of the haplotype and therefore able to maintain nearly normal hematopoiesis for several years. The PNH clone in this patient propagated without loss of HLA alleles, supporting the idea that PNH clones are less susceptible to immune attack even when they express target antigens. HLA-restricted CTLs might have led to clonal selection of GPI (+) cells in our patient, but how the PNH cells in the same patient escaped attack is unknown. 6pLOH in the GPI (−) clone could result from mitotic recombination, but it is still to be clarified if additional CN-6pLOH endows GPI (−) cells with a comparative growth advantage under HLA-restricted immune attack. Clonal evolution in both the GPI (+) and GPI (−) cells may have caused the balanced coexistence with nearly normal blood count. Further analysis would be necessary to examine whether this phenomenon is common in other PNH patients, and assessment of both clones in the patient would be needed. In conclusion, our case supports the hypothesis that a hostile immune environment drives selection of resistant hematopoietic cell clones and indicates that clonal evolution may occur also in normal phenotype (non-PNH) cells in some cases.

Acknowledgements

This research was supported by the Intramural Research Program of the NIH, the NHLBI, and in part by a Grant-in-Aid for Scientific Research from the Ministry of Education, Culture, Sports, Science and Technology of Japan. The authors thank Satoru Hayashi for excellent technical assistance.

Authorship contributions

NSY was the principal investigator and takes primary responsibility for the paper; YU, SK, and NSY designed the research; YU and SK performed the laboratory work for this study; JN, YM, and YK recruited the patients in Japan and provided vital patients samples and clinical information; TK, YK, and NSY coordinated and supervised the study; YU and NSY wrote the manuscript. All authors approved the final version of the manuscript.

Conflict of interest disclosures

The authors report no potential conflict of interest.

References

1. Parker C, Omine M, Richards S, *et al.* Diagnosis and management of paroxysmal nocturnal hemoglobinuria. *Blood* 2005;**106**:3699–709.
2. Takeda J, Miyata T, Kawagoe K, Iida Y, Endo Y, Fujita T, Takahashi M, Kitani T, Kinoshita T. Deficiency of the GPI anchor caused by a somatic mutation of the PIG-A gene in paroxysmal nocturnal hemoglobinuria. *Cell* 1993;**73**:703–11.
3. Araten DJ, Nafa K, Pakdeesuwan K, Luzzatto L. Clonal populations of hematopoietic cells with paroxysmal nocturnal hemoglobinuria genotype and phenotype are present in normal individuals. *Proc Natl Acad Sci USA* 1999;**96**:5209–14.
4. Nagakura S, Ishihara S, Dunn DE, *et al.* Decreased susceptibility of leukemic cells with PIG-A mutation to natural killer cells in vitro. *Blood* 2002;**100**:1031–7.
5. Hanaoka N, Kawaguchi T, Horikawa K, Nagakura S, Mitsuya H, Nakakuma H. Immunoselection by natural killer cells of PIGA mutant cells missing stress-inducible ULBP. *Blood* 2006;**107**:1184–91.
6. Murakami Y, Kosaka H, Maeda Y, Nishimura J, Inoue N, Ohishi K, Okabe M, Takeda J, Kinoshita T. Inefficient response of T lymphocytes to GPI-anchor-negative cells: implications for paroxysmal nocturnal hemoglobinuria. *Blood* 2002;**100**:4116–22.
7. Katagiri T, Sato-Otsubo A, Kashiwase K, *et al.* Frequent loss of HLA alleles associated with copy number-neutral 6pLOH in acquired aplastic anemia. *Blood* 2011;**118**:6601–9.
8. Maciejewski JP, Tiu RV, O'Keefe C. Application of array-based whole genome scanning technologies as a cytogenetic tool in haematological malignancies. *Br J Haematol* 2009;**146**:479–88.

9. Itoh Y, Mizuki N, Shimada T, Azuma F, Itakura M, Kashiwase K, Kikkawa E, Kulski JK, Satake M, Inoko H. High-throughput DNA typing of HLA-A, -B, -C, and -DRB1 loci by a PCR-SSOP-Luminex method in the Japanese population. *Immunogenetics* 2005;**57**:717–29.
10. Shichishima T, Okamoto M, Ikeda K, Kaneshige T, Sugiyama H, Terasawa T, Osumi K, Maruyama Y. HLA class II haplotype and quantitation of WT1 RNA in Japanese patients with paroxysmal nocturnal hemoglobinuria. *Blood* 2002;**100**:22–8.
11. Shichishima T, Noji H, Ikeda K, Akutsu K, Maruyama Y. The frequency of HLA class I alleles in Japanese patients with bone marrow failure. *Haematologica* 2006;**91**:856–7.
12. Karadimitris A, Luzzatto L. The cellular pathogenesis of paroxysmal nocturnal haemoglobinuria. *Leukemia* 2001;**15**:1148–52.
13. Gargiulo L, Papaioannou M, Sica M, *et al.* Glycosylphosphatidylinositol-specific, CD1d-restricted T cells in paroxysmal nocturnal hemoglobinuria. *Blood* 2013;**121**:2753–61.

BJ Biomolecules

Biochem. J. (2014) **463**, 249–256 (Printed in Great Britain) doi:10.1042/BJ20140541

New insights into the functions of PIGF, a protein involved in the ethanolamine phosphate transfer steps of glycosylphosphatidylinositol biosynthesis

Matthew J. STOKES*, Yoshiko MURAKAMI*†, Yusuke MAEDA*†, Taroh KINOSHITA*† and Yasu S. MORITA*†[1]

*Laboratory of Immunoglycobiology, WPI Immunology Frontier Research Center, Osaka University, Osaka 565-0871, Japan
†Department of Immunoregulation, Research Institute for Microbial Diseases, Osaka University, Osaka 565-0871, Japan

PIGF is a protein involved in the ethanolamine phosphate (EtNP) transfer steps of glycosylphosphatidylinositol (GPI) biosynthesis. PIGF forms a heterodimer with either PIGG or PIGO, two enzymes that transfer an EtNP to the second or third mannoses of GPI respectively. Heterodimer formation is essential for stable and regulated expression of PIGO and PIGG, but the functional significance of PIGF remains obscure. In the present study, we show that PIGF binds to PIGO and PIGG through distinct molecular domains. Strikingly, C-terminal half of PIGF was sufficient for its binding to PIGO and PIGG and yet this truncation mutant could not complement the PIGF defective mutant cells, suggesting that heterodimer formation is not sufficient for PIGF function. Furthermore, we identified a highly conserved motif in PIGF and demonstrated that the motif is not involved in binding to PIGO or PIGG, but critical for its function. Finally, we identified a PIGF homologue from *Trypanosoma brucei* and showed that it binds specifically to the *T. brucei* PIGO homologue. These data together support the notion that PIGF plays a critical and evolutionary conserved role in the ethanolamine-phosphate transfer-step, which cannot be explained by its previously ascribed binding/stabilizing function. Potential roles of PIGF in GPI biosynthesis are discussed.

Key words: ethanolamine phosphate transferase, glycosylphosphatidylinositol, membrane protein, metabolism, PIGF, *Trypanosoma brucei*.

INTRODUCTION

Phosphatidylinositol-anchored proteins and glycans are found in evolutionarily diverse organisms including bacteria, protozoa, fungi, plants and animals. The structure of eukaryotic glycosylphosphatidylinositol (GPI) was first revealed by using a GPI-anchored variant surface glycoprotein of *Trypanosoma brucei* in 1985 [1,2]. Since then, structures of GPI-anchored proteins have been reported from many organisms and it has become clear that the core structure of protein-EtNP-6Manα1,2Manα1,6Manα1,4GlcNα1,6*myo*-inositol-phospholipid is highly conserved through the eukaryotic evolution [EtNP (ethanolamine phosphate); Man (mannose); GlcN (glucosamine)] (Figure 1). More than 20 genes involved in the GPI-anchor biosynthesis have been identified [3]. This core structure is modified by a variety of structures such as additional EtNP or mono/oligo-saccharides, but the physiological significance of various modifications in various GPI-anchored proteins remains largely unknown.

An evolutionarily conserved feature of GPI structure in mammalian and yeast cells is that an additional EtNP residue modifies both the first and second mannoses in addition to the third mannose. Phosphatidylinositol glycan anchor biosynthesis, class O (PIGO; Gpi13p in yeast) is involved in the attachment of the core EtNP on to the third mannose [4–6]. The donor of EtNP is phosphatidylethanolamine (PE) [7,8] and its EtNP moiety is transferred to GPI in a transphosphodiesterase reaction. Indeed, PIGO has conserved motifs found in phosphodiesterases and nucleotide pyrophosphatases, suggesting that it has a catalytic function. Homologues of PIGO, namely phosphatidylinositol glycan anchor biosynthesis, class N (PIGN; Mcd4p in yeast) and phosphatidylinositol glycan anchor biosynthesis, class G (PIGG; Gpi7p in yeast), mediate the transfer of EtNP to the first and second mannoses respectively [9–13]. Although the physiological significance of these additional EtNP structures are poorly understood, these steps are critical for GPI-anchor biosynthesis and trafficking. In yeast, a terpenoid lactone, YW3548, which inhibits the enzymatic activity of Mcd4p [9], blocked the addition of the third mannose, suggesting that EtNP needs to be attached to the first mannose before the third mannose transfer occurs [14]. Furthermore, mutation in the *PIGN* gene is associated with defects in forebrain development in mice and an autosomal recessive syndrome in human characterized by dysmorphic features and congenital neurological abnormalities [15–17]. *GPI7* is not an essential gene in yeast and a GPI-intermediate lacking an EtNP attachment mediated by Gpi7p can still be transferred to proteins [11,13]. Nevertheless, yeast GPI7 has been implicated in cell separation and subsequent growth of daughter cells [18]. More recently, we demonstrated in mammalian cells that the second EtNP added by PIGG is removed in the endoplasmic reticulum (ER) by a phosphodiesterase, PGAP5, soon after attachment to

Abbreviations: ALDH, acetaldehyde dehydrogenase; CHO, Chinese-hamster ovary; ER, endoplasmic reticulum; EtNP, ethanolamine phosphate; GlcN, glucosamine; GPI, glycosylphosphatidylinositol; PE, phosphatidylethanolamine; PIG, phosphatidylinositol glycan anchor biosynthesis; TM, transmembrane, WT, wild-type.

[1] To whom correspondence should be addressed at the present address: Department of Microbiology, University of Massachusetts, Amherst, MA 01003, U.S.A. (email ymorita@microbio.umass.edu).

Table 1 Primers used in the present study

Name	Forward primer sequence (5′→3′)	Reverse primer sequence (5′→3′)
PIGF-ΔN1	AAAACTGCAGGACTACAAGGACGACGATGACAAGGTCGACGAGAACTTCTCAATATTG	ATAGTTTAGCGGCCGCTTAATTGTTCTTGTATGT
PIGF-ΔN2	AAAACTGCAGCCACCATGGACTACAAGGACGACGATGACAAGGTCGACAAACCAAATACATCCTCT	ATAGTTTAGCGGCCGCTTAATTGTTCTTGTATGT
PIGF-ΔN3	AAAACTGCAGGACTACAAGGACGACGATGACAAGGTCGACTATGGAGCACCACTGATA	ATAGTTTAGCGGCCGCTTAATTGTTCTTGTATGT
PIGF-ΔC1	AAAACTGCAGCCACCATGGACTACAAGGACGACGATGACAAGGTCGACAAAGATAACGATATCAAG	ATAGTTTAGCGGCCGCTTACGTACAGGAGATGGGCCA
PIGF-ΔC2	AAAACTGCAGCCACCATGGACTACAAGGACGACGATGACAAGGTCGACAAAGATAACGATATCAAG	ATAGTTTAGCGGCCGCTTACTGGAGACTATTCTCCCA
PIGF-ΔC3	AAAACTGCAGCCACCATGGACTACAAGGACGACGATGACAAGGTCGACAAAGATAACGATATCAAG	ATAGTTTAGCGGCCGCTTATGTTTCCAATGCCAACTC
PIGF-ΔN1ΔC1	AAAACTGCAGGACTACAAGGACGACGATGACAAGGTCGACGAGAACTTCTCAATATTG	ATAGTTTAGCGGCCGCTTACGTACAGGAGATGGGCCA
TbPIGF	ACGCGTCGACGTTCTTTGGGTAGTTATTTTCTCACTCGCT	ATAGTTTAGCGGCCGCTTATTCCACCTTTTCATCAACCTTCTCTGGT
TbPIGO	CCGGAATTCCCACCATGACCTCACGCTCTGAT	CGACGCGTTGCCAGTAACGCAGC

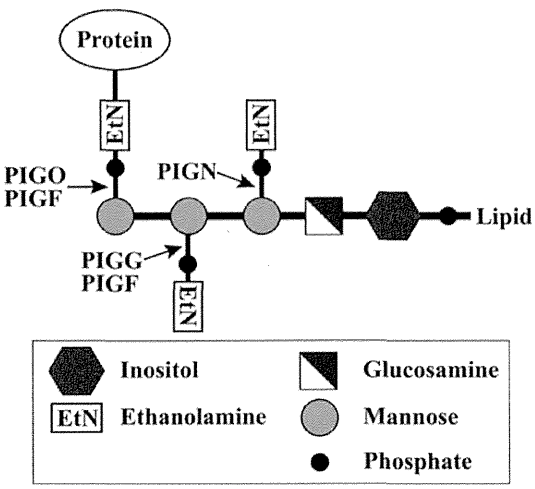

Figure 1 Structure of GPI-anchor core glycan and enzymes involved in the biosynthesis

proteins and suggested that EtNP attached to the second mannose regulates GPI-anchored protein transport in the early secretory pathway [19].

Phosphatidylinositol glycan anchor biosynthesis, class F (PIGF) is another protein involved in EtNP transfer steps of GPI biosynthesis. It is an extremely hydrophobic protein made of 219 amino acid residues in the case of human PIGF [20]. Six transmembrane (TM) domains, identified using the programs SOSUI [21] and TMHMM [22], are distributed through the entire protein. PIGF was initially identified as a protein involved in the addition of the third mannose [4]. Indeed, PIGF binds to PIGO, and PIGO quickly degrades in the absence of PIGF, indicating that PIGF is important for stable expression of PIGO [4]. Interestingly, PIGF binds not only to PIGO but also to PIGG and the stable expression of PIGG is also dependent on PIGF [10]. These observations suggested that PIGF is a critical protein that allows stable expression of the two EtNP transferases, PIGO and PIGG. Nevertheless, we know little about whether PIGF plays this stabilizing role and how the presence of PIGF is critical when co-ordination of multiple EtNP transferases is necessary. In the present paper, we provide evidence that PIGF uses distinct amino acid domains to interact with PIGO or PIGG. Furthermore, we demonstrate that PIGF plays an additional function that cannot be explained by its binding to PIGO or PIGG. Finally, whereas a protozoan parasite *T. brucei* lacks PIGG, we demonstrate the presence of a PIGF homologue, designated as TbPIGF, and its interaction with TbPIGO, indicating that evolution of PIGF is not dependent on the presence of PIGG.

EXPERIMENTAL

Cells and culturing

EL4 class F cells [20], a murine thymoma Thy-1-deficient cell-line, were grown in Dulbecco's modified Eagle's medium supplemented with 10% FBS. Chinese-hamster ovary (CHO)-K1 cells were cultured in Ham's F12 medium supplemented with 10% FBS.

Cloning, preparation of mutant constructs and transfection

Primer sets used to create PIGF mutants are shown in Table 1. Amplified PCR fragments were digested with PstI and NotI and ligated into pMEPyori_puro-FLAG-CD59 vector to generate PIGF proteins with an N-terminal FLAG tag [23]. PIGO and PIGG with an N-terminal GST tag were generated previously [4,10]. *TbPIGF* and *TbPIGO* genes were amplified and cloned into either pMEPyori_puro-FLAG-CD59 or pMEpyori4gGST expression vector. Site-directed mutagenesis was performed as described previously [23]. For transfection of EL4 class F cells, cells were grown to a density of 3×10^6 cells/ml, and 1×10^7 cells were electroporated with 20 μg of plasmid at 1000 μF and 250 V in 0.4 mm gap cuvette. The cells were then transferred to 10 ml of Eagle's medium containing 10% FBS and cultured for 2 days. For CHO-K1 cells, 1×10^7 cells were electroporated with 20 μg of plasmid at 1000 μF and 250 V in 0.4 mm gap cuvette. The cells were then transferred to 10 ml of Ham's F12 medium containing 10% FBS and cultured for 2 days.

Fluorescence staining and FACS analysis

Surface-expressed Thy-1 was stained by incubating cells with phycoerythrin-conjugated anti-CD90.2 antibody (Becton Dickinson) for 1 h on ice. Stained cells were analysed using a FACScan cytometer (Becton Dickinson).

Immunoprecipitation and Western blotting

Washed cells were resuspended in 0.8 ml of lysis buffer (50 mM Tris/HCl, pH 7.5, 150 mM NaCl, 1% digitonin, 5 mM EDTA and protease inhibitor cocktail) and lysed for 1 h at 4°C. The lysate was then centrifuged at 20000 ***g*** for 15 min to remove cell debris and the supernatant was incubated with glutathione–Sepharose 4B (GE Healthcare) or anti-FLAG M2 Affinity Gel

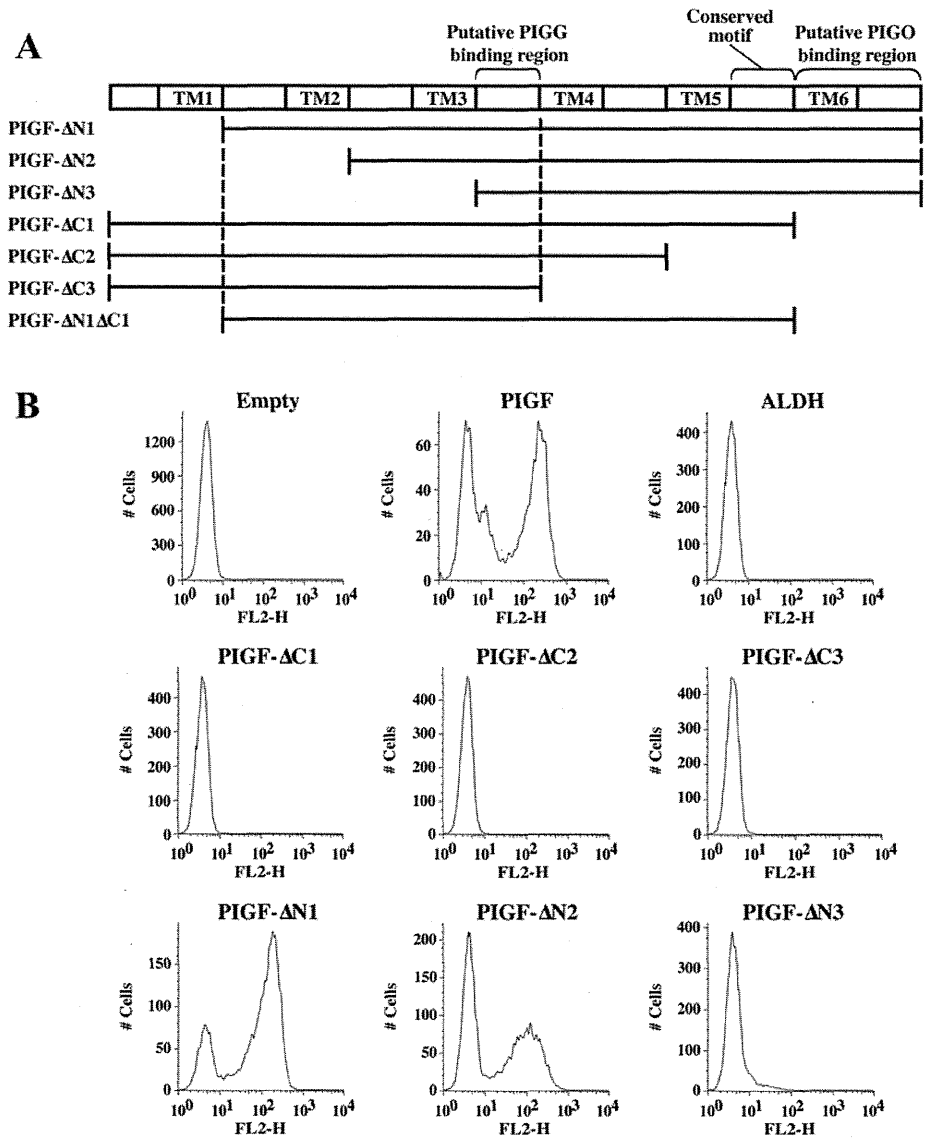

Figure 2 Complementation of PIGF-deficient cells with truncated PIGF

(**A**) Schematic representation of PIGF depicting predicted TM domains and areas of truncation in the tested constructs, binding regions and the location of the conserved motif. (**B**) EL4 class F cells were transiently transfected with the truncated PIGF constructs and tested for surface expression of Thy-1.

(Sigma). The beads were washed and bound proteins were eluted with reduced glutathione or FLAG peptide respectively. We often performed sequential pull-downs (e.g. glutathione–Sepharose pull-down and then anti-FLAG immunoprecipitation as in Figure 3) to collect unbound proteins in the initial pull-down. The eluted samples were then denatured in a sample loading buffer under reducing conditions for 1 h at 4 °C and proteins were separated by SDS/PAGE (15 % or 10–20 % gradient gel). Proteins were transferred on to PVDF membranes (Millipore) for Western blotting. Primary antibodies were mouse anti-FLAG M2 monoclonal antibody (Sigma) or goat anti-GST polyclonal antibody (GE Healthcare). For secondary antibody, horseradish peroxidase-conjugated goat anti-mouse IgG (Cell Signaling Technology) was used and the protein bands were visualized by chemiluminescence using ECL-Plus (GE Healthcare).

RESULTS

Functional domains of human PIGF

To further examine the interaction of PIGF with its binding partners, PIGO and PIGG, a series of truncated mutants were created (Figure 2A). ORFs were created to incorporate a FLAG tag at the N-terminus for constructs PIGF-ΔN2, PIGF-ΔC1, PIGF-ΔC2 and PIGF-ΔC3 and cloned in the pMEpyori vector. In order to maintain the correct orientation for constructs PIGF-ΔN1, PIGF-ΔN3 and PIGF-ΔN1ΔC1, an ORF was generated

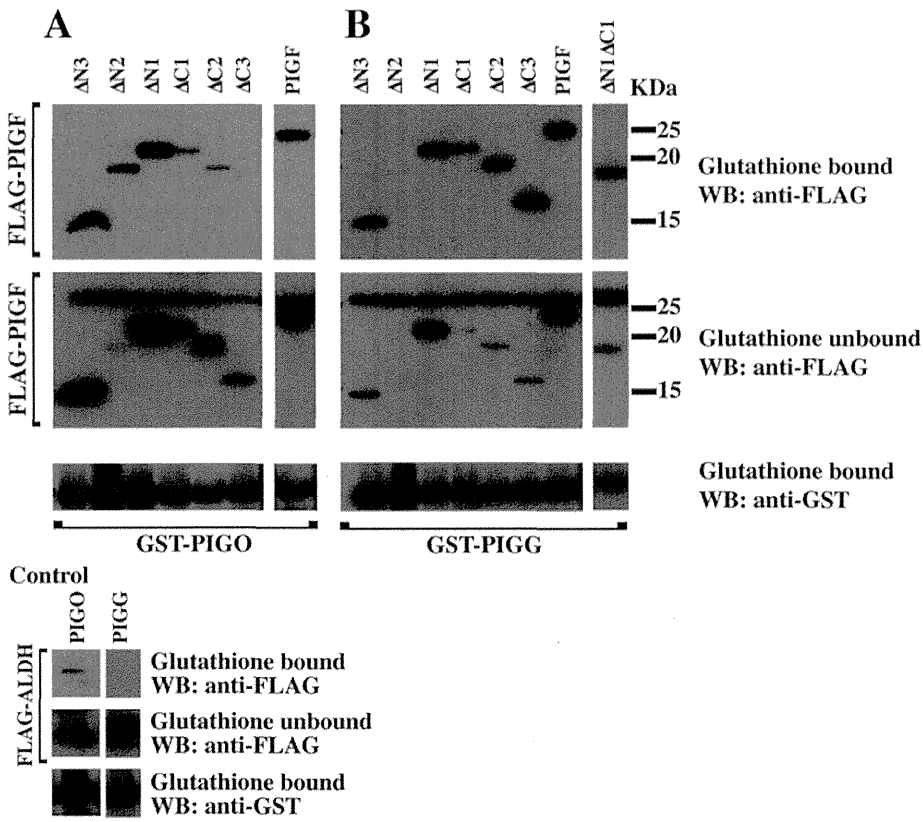

Figure 3 Binding of truncated PIGFs with PIGO and PIGG

CHO-K1 cells co-expressing WT FLAG–PIGF, truncated FLAG–PIGF or FLAG–ALDH with GST–PIGO (**A**), or GST–PIGG (**B**), were lysed in 1 % digitonin. The GST-tagged proteins in the supernatant were precipitated using glutathione beads. Unbound FLAG-tagged proteins were then precipitated with anti-FLAG–agarose. GST-tagged (bottom panels) and co-precipitated FLAG-tagged proteins (top panels) were detected by Western blot analysis using anti-GST and anti-FLAG respectively. Unbound FLAG-tagged proteins were detected using anti-FLAG antibody (middle panel). The top band constantly appearing in the middle panel is IgG light chain released during anti-FLAG immunoprecipitation.

and ligated directly into a pMEpyori containing a cleavable ER import sequence and a FLAG tag at the N-terminus [23]. To test the function of the truncated PIGF mutants, the constructs were transiently transfected into an EL4 murine thymoma cell line that lacks the surface expression of GPI-anchored proteins, such as Thy-1, due to PIGF deficiency (class F cells) [20]. Restoration of Thy-1 expression by each PIGF mutant was determined using FACS analysis (Figure 2B), and used as an indication of PIGF function. As controls, full length PIGF could restore the surface expression of Thy-1, whereas an unrelated membrane protein, acetaldehyde dehydrogenase (ALDH) had no effect on the Thy-1 expression. The removal of the C-terminal TM domain TM6 (PIGF-ΔC1) resulted in complete loss of PIGF's ability to restore Thy-1 expression in the class F cells, indicating that the C-terminal 31 amino acid residues are critical for the function or the structural integrity of PIGF. In contrast, the N-terminal two TM domains (TM1 and TM2) were not an absolute requirement for PIGF function because PIGF-ΔN1 and PIGF-ΔN2 can at least partially restore the expression of Thy-1. Further deletion (PIGF-ΔN3) abolished PIGF's ability to restore Thy-1 expression, suggesting that amino acid residues beyond position 63 carry critical residues for PIGF function. Taken together, although TM1 and TM2 are dispensable for PIGF function, the remaining C-terminal regions appear to be critical for its function.

PIGF forms heterodimers with either PIGO or PIGG and stabilizes these EtNP transferases, thereby partaking in GPI biosynthesis. We therefore wondered whether these truncated PIGF mutants lost their ability to restore Thy-1 expression because they can no longer bind to these binding partners. To test this, the truncated FLAG–PIGFs (and FLAG–ALDH as a control) were transiently co-expressed in CHO-K1 cells with GST-tagged PIGO or PIGG. The GST-tagged proteins were then immunoprecipitated with glutathione–Sepharose beads from digitonin-lysed cells and analysed for the co-immunoprecipitation of PIGF or ALDH by Western blotting. We have previously established that complexes of GPI biosynthetic enzymes are maintained in digitonin-lysed cells, but not in Nonidet P40-lysed cells [24] and successfully used ALDH, an ER-resident membrane protein as a negative control for immunoprecipitation. In the present study, we first showed that full-length PIGF binds to both PIGO and PIGG as positive controls and that ALDH binds to neither PIGO nor PIGG as negative controls (Figure 3). Figure 3(A) shows the results of co-immunoprecipitation with PIGO and indicates that the removal of the C-terminal TM domain (ΔC1, ΔC2 and ΔC3) resulted in little recovery of PIGF (upper panel). The inefficient recovery is not due to poor expression of these mutant proteins because these mutant proteins can be recovered by immunoprecipitation of unbound fractions using anti-FLAG affinity beads (lower panel). Therefore

the inability of PIGF-ΔC1, PIGF-ΔC2 and PIGF-ΔC3 to bind to PIGO is consistent with their loss of ability to restore Thy-1 expression in EL4 class F cells (see Figure 2B). These data suggest that the C-terminal TM domain is essential for PIGO binding. In contrast, the removal of the N-terminal three TM domains had no effect on PIGO binding (Figure 3A). In particular, PIGF-ΔN3 can efficiently bind to PIGO even though this construct could not restore the mutant phenotype of EL4 class F cells (see Figure 2B). These results indicate that binding of PIGF to PIGO may not be sufficient for the function of PIGF.

Because PIGF can also bind to PIGG, the inability of PIGF-ΔN3 to restore the mutant phenotype of EL4 class F cells may be attributed to its binding property to PIGG. We therefore transiently expressed the truncated FLAG–PIGFs (and FLAG–ALDH as a control) in CHO-K1 cells together with GST–PIGG. We, additionally, made a truncation mutant lacking both terminal TM domains (TM1 and TM6), designated PIGF-ΔN1ΔC1. Surprisingly, all truncated PIGFs were able to bind PIGG (Figure 3B). Because all truncated mutants contain the region between TM3 and TM4, this region may be critical for the interaction of PIGF to PIGG.

In order to clarify further the role of the C-terminal region in PIGO binding, the known PIGF amino acid sequences from various organisms were analysed. We identified a highly conserved amino acid motif consisting of the consensus PLDWxRxWQxWP (Figure 4A, red bar). To test the importance of this motif, FLAG–PIGF ORFs containing point mutations of these residues were generated and their ability to restore Thy-1 expression in class F cell was tested by FACS analysis. Only the mutations pertaining to Leu^{175} and Asp^{176} were unable to fully restore expression (Figure 4B) and point mutations W177A, Q182A, W184A and P185A were still able to restore Thy-1 expression (not shown). The importance of hydrophobicity of the leucine residue at position 175 was demonstrated by the comparison with L175K and L175A restoration effect. The effect of a positively charged lysine residue at position 175 greatly retarded Thy-1 restoration when compared with a hydrophobic alanine residue. The importance of an aspartic acid residue at position 176 was not entirely dependent on its negative charge because mutations to another negatively charged amino acid glutamic acid (D176E), positively charged amino acid lysine (D176K) or hydrophobic amino acid alanine (D176A) all showed similar reduction in surface expression of GPI-anchored proteins compared with wild-type (WT) PIGF. The combined mutation L175K/D176K had a cumulative effect and almost completely abolished PIGF's ability to restore Thy-1 expression in class F cells, indicating that these two positions are critical for the function of PIGF.

We wanted to test whether the conserved amino acids are critical for the interaction of PIGF to PIGO or PIGG. Therefore all FLAG–PIGF point mutants were co-expressed with GST–PIGO or GST–PIGG in CHO-K1 cells and immunoprecipitated using glutathione–Sepharose. All point mutants were able to bind both PIGO (Figure 4C) and PIGG (Figure 4D). Taken together, these results indicate that a conserved motif present in the C-terminal cytoplasmic loop of PIGF is functionally important, but is not involved in binding to PIGO or PIGG.

Identification of *T. brucei* PIGF and PIGO homologues

To provide insight into the evolutionary conservation of PIGF, we took advantage of the newly identified functional motif of PIGF. We used $LDW(X)_4QXWP$ as query to search the non-redundant protein sequence database at NCBI for potential PIGF homologues in other organisms. We identified a limited distribution of this motif outside of fungi, green plants and metazoans. Among these, we identified PIGF homologues in kinetoplastids (Figure 5A). The putative ORF in *T. brucei* was identified as *TbPIGF* Tb927.10.12010 (GeneID 3662199). *TbPIGF* encodes a 131-amino-acid protein with three putative TM domains. Based on amino acid sequence alignment, TbPIGF was 20.1 % identical with human PIGF.

To examine whether TbPIGF functions to bind TbPIGO, we first identified TbPIGO based on its homology with human PIGO. The putative gene *TbPIGO* (Tb927.11.5070) was cloned into a plasmid to express GST-tagged TbPIGO. This construct was transiently transfected together with a plasmid to express FLAG-tagged TbPIGF in CHO-K1 cells (Figure 5B). We then performed immunoprecipitation to examine whether TbPIGF binds to TbPIGO. We found that TbPIGF can specifically bind to TbPIGO and not to human PIGO. In contrast, human PIGF was promiscuous in that it binds to both human PIGO and TbPIGO. As a negative control, unrelated ALDH did not bind to human PIGO or TbPIGO. These data showed that TbPIGF was able to bind TbPIGO *in vivo*, further supporting a similar role for TbPIGF played in the GPI biosynthesis in *T. brucei*.

As expression and binding of TbPIGO and TbPIGF were efficient in mammalian cells, the ability of TbPIGF and TbPIGO to function in mammalian cells was tested. TbPIGF and TbPIGO were expressed alone or in combination with their mammalian binding counterpart in PIGF- and PIGO-deficient cells. The expression of these proteins failed to restore the expression of Thy-1, suggesting that they were not functional in mammalian cells (results not shown).

DISCUSSION

It was once postulated that PIGF may be an EtNP transferase [20]. However, subsequent studies demonstrated that PIGN, PIGG and PIGO are catalytic components of EtNP transferases and PIGF came to be considered as a stabilizing factor [4,10]. Our current study suggests a new additional role for PIGF, which cannot be explained by its structural role of forming heterodimers with PIGO or PIGG and stabilizing these catalytic subunits.

Two lines of evidence support our conclusion that the newly identified function of PIGF is beyond its stabilizing role. First, a truncated form of PIGF, PIGF-ΔN3, which lacks the N-terminal half of the protein, lost its functional ability to restore the surface expression of GPI-anchored proteins in a PIGF-deficient mutant (see Figure 2B), even though PIGF-ΔN3 can still bind to both PIGO and PIGG (see Figure 3). We believe that PIGF binding stabilizes PIGO and PIGG, but our data suggest that stable heterodimer formation is not sufficient for the function of PIGF. Secondly, we identified Leu^{175} and Asp^{176} as highly conserved amino acid residues critical for the function of PIGF. Double point mutation of L175K/D176K resulted in ablation of PIGF's ability to restore the surface expression of GPI-anchored proteins in a PIGF-deficient mutant (see Figure 4B). Nevertheless, the double point mutant was able to form a complex with both PIGO and PIGG, indicating again that PIGF plays a functional role that cannot be explained by binding and stabilizing PIGO and PIGG.

What is the function of PIGF? We proposed previously that the quantity of PIGF is limiting and relative activities of PIGG and PIGO are partially dictated by the availability of PIGF [10]. This scenario is based on the ability of PIGF to stably form a complex with either PIGO or PIGG, but not both, thereby controlling the relative activities of these enzymes. To consider